

**IDENTIFICATION OF NOVEL 14-3-3 SIGMA  
HOMODIMER STABILISER IN  
NASOPHARYNGEAL CARCINOMA**

**GHAZI AHMAD AL JABAL**

**UNIVERSITI SAINS MALAYSIA**

**2023**

**IDENTIFICATION OF NOVEL 14-3-3 SIGMA  
HOMODIMER STABILISER IN  
NASOPHARYNGEAL CARCINOMA**

by

**GHAZI AHMAD AL JABAL**

**Thesis submitted in fulfilment of the requirements  
for the degree of  
Doctor of Philosophy**

**September 2023**

## ACKNOWLEDGEMENT

I would like to express my sincere gratitude to my supervisor, Dr. Beow Keat Yap, for his guidance, support, and encouragement throughout my PhD journey. His expertise and dedication have been invaluable in shaping my research and his patience and understanding have been a constant source of motivation. I am deeply grateful for his time and effort in reviewing my work and providing valuable feedback. I would not have been able to complete this thesis without his unwavering support and guidance. I extend my heartfelt thanks to him.

I would like to extend my sincerest gratitude to my co-supervisor, Dr Teh Aik Hong, for his invaluable contributions to my PhD research. His guidance, support and constant encouragement were essential in the successful completion of my thesis. His willingness to provide me full access to the CCB labs and his continuous help, support and follow-up throughout the research process was greatly appreciated. Thank you, Dr Teh, for your time and help.

I am deeply grateful for the invaluable support and contributions provided by my colleague, Melissa, throughout my research. Melissa provided technical assistance and helpful guidance in the genomic lab, and her willingness to share her knowledge and experience made the process much smoother and more efficient. Furthermore, I would like to extend my appreciation to my colleagues, Dickson and Fei Her, for their outstanding contributions to our team. Their expertise and knowledge in the field were invaluable to me, and their positive attitude and friendly demeanour always made me feel welcome. Working alongside Melissa, Dickson, and Fei Her has been an incredible opportunity, and I am truly thankful for their support and impact on my academic journey.

I am deeply grateful to my colleagues and best friends, Ahmed Yaseen, Mohammad Althiabat, Mohammed Dayoob, Bilal Alrimawi, Abdulsalam Qahtan, Nadeem AL Ameen, for their support, positive attitudes, and valuable advice throughout my PhD journey. Their friendship has not only provided a comfortable and motivating environment, but it has also been a source of constant inspiration. Their willingness to listen, help and provide valuable advice has been invaluable, their encouragement and support during times of stress have been an essential part of my success. The support and guidance provided by these friends have played a crucial role in my personal and professional growth.

I would like to express my deepest gratitude to my parents for their unwavering love, support, and throughout my entire academic journey. Their encouragement and belief in me have been a constant source of motivation and inspiration. I could not have achieved this milestone without their guidance and sacrifices. I am forever grateful for all that they have done for me and for the countless ways they have made this journey possible. This thesis is a testament to their investment in my success and I dedicate it to them with all my love and appreciation.

Last but not least, I would like to express my sincerest gratitude to my wife, Eng. Balqees Alhouran, for her unwavering love and support. Her understanding, patience, constant encouragement, and sacrifices during this time have been invaluable and I could not have done it without her. I would also like to thank my children, Ahmad and Mohammad, for their love and support. They have been my constant source of joy and inspiration throughout this journey. Their laughter and playfulness have helped me to lighten up the moments of stress and their presence in my life is my greatest treasure. I am truly blessed to have their love and support, and this thesis is dedicated to my loving family.

## TABLE OF CONTENTS

<b>ACKNOWLEDGEMENT</b> .....	<b>ii</b>
<b>TABLE OF CONTENTS</b> .....	<b>iv</b>
<b>LIST OF TABLES</b> .....	<b>ix</b>
<b>LIST OF FIGURES</b> .....	<b>xi</b>
<b>LIST OF SYMBOLS</b> .....	<b>xxi</b>
<b>LIST OF ABBREVIATIONS</b> .....	<b>xxii</b>
<b>ABSTRAK</b> .....	<b>xxiv</b>
<b>ABSTRACT</b> .....	<b>xxvi</b>
<b>CHAPTER 1 INTRODUCTION</b> .....	<b>1</b>
1.1 Background of the study .....	1
1.1.1 Nasopharyngeal carcinoma (NPC).....	1
1.1.2 14-3-3 $\sigma$ (Stratifin, or Sfn) .....	2
1.1.3 Structure of 14-3-3 $\sigma$ .....	5
1.1.4 Role of 14-3-3 $\sigma$ in cancer .....	9
1.1.5 Expression of 14-3-3 $\sigma$ in NPC.....	11
1.2 Problem Statement .....	13
1.3 Objectives.....	14
1.4 Scope of the thesis.....	14
<b>CHAPTER 2 LITERATURE REVIEW</b> .....	<b>17</b>
2.1 Introduction .....	17
2.2 Current status and outlook of drug discovery research against 14-3-3 $\sigma$ .....	17
2.2.1 14-3-3 protein-protein interaction (PPI) modulators.....	17
2.2.1(a) 14-3-3 $\sigma$ PPI stabilisers.....	18
2.2.1(b) 14-3-3 $\sigma$ PPI inhibitors .....	29
2.2.1(c) Summary and outlook of 14-3-3 $\sigma$ PPI modulators.....	40

2.2.2	14-3-3 $\sigma$ homodimer stabilisers .....	41
2.3	Computer-Aided Drug Design (CADD) in drug discovery .....	42
2.3.1	The trend of drug discovery and development.....	42
2.3.2	CADD in drug discovery .....	42
2.3.2(a)	Molecular docking.....	43
2.3.2(b)	Molecular dynamic simulation .....	47
2.4	Biophysical techniques in drug discovery.....	52
2.4.1	Protein-ligand interaction studies.....	52
2.4.2	Protein stability studies .....	55
<b>CHAPTER 3 METHODOLOGY.....</b>		<b>57</b>
3.1	Introduction .....	57
3.2	General materials .....	59
3.2.1	Chemical reagents .....	59
3.2.2	Bacterial strain .....	59
3.2.3	Plasmid.....	59
3.2.4	Bacterial media.....	60
3.2.5	Buffers and solutions .....	60
3.2.6	Instrument/Software.....	61
3.2.7	Web resources .....	63
3.3	General methods.....	64
3.3.1	<i>In silico</i> design and prediction of potential 14-3-3 $\sigma$ homodimer stabilisers.....	64
3.3.1(a)	Protein preparation .....	64
3.3.1(b)	Ligand preparation.....	64
3.3.1(c)	Receptor grid map generation for molecular docking. ....	65
3.3.1(d)	Molecular docking.....	65
3.3.1(e)	Analysis of the docking results.....	66

3.3.1(f)	Molecular dynamics simulations.....	66
3.3.2	Synthesis, purification and characterisation of selected potential 14-3-3 $\sigma$ homodimer stabilisers .....	67
3.3.2(a)	Dipeptide analogues synthesis.....	67
3.3.2(b)	Dipeptide analogues purification and characterisation.....	71
3.3.3	Expression, purification and characterisation of 14-3-3 $\sigma$ protein .....	72
3.3.3(a)	Plasmid isolation.....	72
3.3.3(b)	Preparation of <i>E. coli</i> BL21 (DE3) competent cells.....	72
3.3.3(c)	Plasmid transformation.....	73
3.3.3(d)	N-GST-14-3-3 $\sigma$ protein expression.....	74
3.3.3(e)	Cell lysis by sonication.....	74
3.3.3(f)	N-GST-14-3-3 $\sigma$ protein purification .....	74
3.3.3(g)	GST-tag cleavage from N-GST-14-3-3 $\sigma$ fusion protein and purification of 14-3-3 $\sigma$ protein.....	75
3.3.3(h)	Polyacrylamide gel electrophoresis (PAGE) analysis .....	75
3.3.3(i)	Characterisation of the purified 14-3-3 $\sigma$ protein.....	76
3.3.4	<i>In vitro</i> binding interaction studies .....	77
3.3.4(a)	[ <sup>1</sup> H]-Carr-Purcell-Meiboom-Gill (CPMG) NMR experiment .....	77
3.3.4(b)	Isothermal titration calorimetry (ITC).....	77
3.3.5	<i>In vitro</i> stabilisation studies by dynamic light scattering (DLS) .....	78
<b>CHAPTER 4 RESULTS .....</b>		<b>79</b>
4.1	<i>In silico</i> design and prediction of potential 14-3-3 $\sigma$ homodimer stabilisers..	79
4.1.1	The cavity at the dimer interface of 14-3-3 $\sigma$ as a putative druggable pocket.....	79
4.1.2	Small molecules as potential 14-3-3 $\sigma$ homodimer stabilisers.....	81
4.1.3	GCP-Lys-OMe as a potential 14-3-3 $\sigma$ homodimer stabiliser .....	85

4.1.4	Dipeptide analogues as potentially novel 14-3-3 $\sigma$ homodimer stabilisers.....	105
4.2	Synthesis, purification and characterisation of potentially novel 14-3-3 $\sigma$ homodimer stabilisers .....	120
4.3	Expression, purification and characterisation of 14-3-3 $\sigma$ protein.....	125
4.4	<i>In vitro</i> binding interaction studies .....	129
4.4.1	Validation of the peptide analogues binding on 14-3-3 $\sigma$ by [ <sup>1</sup> H]-Carr-Purcell-Meiboom-Gill (CPMG) NMR experiment .....	129
4.4.2	Estimation of the binding affinity of Peptide 3 on 14-3-3 $\sigma$ by isothermal titration calorimetry (ITC).....	132
4.5	<i>In vitro</i> stabilisation studies of 14-3-3 $\sigma$ by Peptide 3 using dynamic light scattering (DLS) .....	133
<b>CHAPTER 5 DISCUSSION .....</b>		<b>137</b>
5.1	<i>In silico</i> design and prediction of potential 14-3-3 $\sigma$ homodimer stabilisers	137
5.1.1	The cavity at the dimer interface of 14-3-3 $\sigma$ is a putative druggable pocket.....	137
5.1.2	Compound III is a potential small molecule 14-3-3 $\sigma$ homodimer stabilisers .....	138
5.1.3	GCP-Lys-OMe is a potential 14-3-3 $\sigma$ homodimer stabiliser.....	138
5.1.4	Peptide 3 is a potentially novel 14-3-3 $\sigma$ homodimer stabiliser....	144
5.1.5	The <i>in silico</i> designed peptides as selected compounds for subsequent <i>in vitro</i> studies .....	147
5.2	Synthesis, purification and characterisation of potentially novel 14-3-3 $\sigma$ homodimer stabilisers .....	148
5.2.1	The designed peptide analogues are successfully synthesised with sufficient purity .....	148
5.3	Expression, purification and characterisation of 14-3-3 $\sigma$ protein.....	149
5.3.1	The recombinantly expressed full-length human 14-3-3 $\sigma$ is sufficiently pure and correctly folded .....	149
5.4	<i>In vitro</i> binding interaction studies .....	151
5.4.1	The dipeptide analogues 3, 5, 9, and 19 are able to bind to the 14-3-3 $\sigma$ as predicted <i>in silico</i> .....	151
5.4.2	Peptide 3 only binds weakly to the 14-3-3 $\sigma$ protein .....	153



5.5	<i>In vitro</i> stabilisation studies by dynamic light scattering (DLS).....	154
5.5.1	Peptide 3 is able to stabilise the 14-3-3 $\sigma$ homodimer <i>in vitro</i> .....	154
<b>CHAPTER 6 CONCLUSION AND FUTURE RECOMMENDATIONS....</b>		<b>156</b>
6.1	Conclusion.....	156
6.2	Limitations of the study .....	157
6.3	Recommendations for Future Research .....	158
<b>REFERENCES.....</b>		<b>159</b>
<b>LIST OF PUBLICATIONS</b>		

## LIST OF TABLES

	<b>Page</b>
Table 2.1	Comparison between different types of 14-3-3 $\sigma$ inhibitors ..... 38
Table 3.1	Buffers and solutions used in this study. Amount to add to prepare 1 L buffer with stated compositions are given. .... 60
Table 3.2	Software used in this study. .... 61
Table 3.3	Instrument used in this study. .... 62
Table 3.4	Web resources used in this study. .... 63
Table 3.5	An example of a method used for purification of the peptide by RP-HPLC. .... 71
Table 3.6	An example of a method used for LC-MS analysis of the dipeptides. .... 72
Table 3.7	Composition of SDS-PAGE gel..... 76
Table 4.1	Hydrogen bond pairs between monomers of 14-3-3 $\sigma$ in apo and GCP-Lys-OMe-bound systems at 100 ns simulation. Only the residues at H1-H4 (the dimer interface) are shown. Similar pairs (i.e. involving the same residues) between the two systems are bolded..... 101
Table 4.2	Hydrogen bond occupancy ( $\geq 10\%$ ) between monomers of 14-3-3 $\sigma$ in apo system throughout the whole 100 ns simulation. Only the residues at H1-H4 (the dimer interface) are shown. .... 102
Table 4.3	Hydrogen bond occupancy ( $\geq 10\%$ ) between monomers of 14-3-3 $\sigma$ in GCP-Lys-OMe-bound systems throughout the whole 100 ns simulation. Only the residues at H1-H4 (the dimer interface) are shown. .... 103
Table 4.4	Hydrogen bond occupancy ( $\geq 10\%$ ) between monomers of 14-3-3 $\sigma$ and GCP-Lys-OMe in GCP-Lys-OMe-bound systems

	throughout the whole 100 ns simulation. Only the residues at H1-H4 (the dimer interface) are shown.....	104
Table 4.5	Peptide sequence of the designed dipeptide analogous, along with their predicted binding free energy from focus docking on the dimer cavity of 14-3-3 $\sigma$ protein. The lowest binding free energy peptide in each category is highlighted in gray. ....	105
Table 4.6	Number of residue pairs between monomers with at least 10% hydrogen bond occupancy (14-3-3 $\sigma$ /Peptide 3 complex).....	118
Table 4.7	Number of residue pairs between Peptide 3 and 14-3-3 $\sigma$ with at least 10% hydrogen bond occupancy.....	119

## LIST OF FIGURES

	<b>Page</b>
Figure 1.1	Sequence alignment of the seven human 14-3-3 isoforms (UniProtKB codes, h14-3-3 $\epsilon$ : P62258; h14-3-3 $\sigma$ : P31947; h14-3-3 $\gamma$ : P61981; h14-3-3 $\eta$ : Q04917; h14-3-3 $\tau$ : P27348; h14-3-3 $\zeta$ : P63104; h14-3-3 $\beta$ : P31946), as performed with ClustalW and ESPrpt 3.0, with red box, white character: strict identity; red character: similarity in group; blue frame: similarity across group. The $\alpha$ -helical regions are indicated above the sequence.....4
Figure 1.2	Phylogenetic tree of the seven human 14-3-3 isoforms generated using ClustalOmega.....4
Figure 1.3	Crystal structures of the seven human 14-3-3 isoforms (PDB codes, h14-3-3 $\beta$ : 6A5Q; h14-3-3 $\gamma$ : 2B05; h14-3-3 $\epsilon$ : 2BR9; h14-3-3 $\eta$ : 2C63; h14-3-3 $\zeta$ : 1QJA; h14-3-3 $\sigma$ : 1YWT; h14-3-3 $\tau$ : 2BTP) (presented as ribbon) with their peptide ligands (presented as stick, backbone colour white) bound to the amphipathic binding groove of both monomers. ....5
Figure 1.4	Surface representations of the 14-3-3 $\sigma$ homodimer (PDB: 1YWT). The conserved residues are highlighted in yellow colour. The second and third structures are rotated 90° and 180°, respectively, around the x-axis from the previous structure. ....6
Figure 1.5	(a) 14-3-3 $\zeta$ /phosphopeptide complex (mode I, PDB: 1QJB), (b) 14-3-3 $\zeta$ /phosphopeptide complex (mode II, PDB: 1QJA), (c) 14-3-3 $\sigma$ /TASK3 peptide (mode III, PDB: 6GHP). ....8
Figure 1.6	Surface representations of the 14-3-3 $\sigma$ homodimer (PDB: 1YZ5). The amphipathic binding grooves are indicated by blue triangles.....9
Figure 2.1	(a) Chemical structure of fusicoccin-A (FC-A). Three-dimensional (3D) crystal structure of P53/14-3-3 $\sigma$ complex (b) in the absence of FC-A (PDB: 5MOC) and (c) in the presence of FC-A (PDB:

	5MXO), revealed that the C-terminus of the P53 peptide cannot be observed upon binding of FC-A (dashed circles). ....	19
Figure 2.2	(a) Chemical structure of FC-THF. (b) 3D complex of 14-3-3 $\sigma$ /TASK-3 with FC-THF (PDB: 3SMN) revealed hydrophobic (purple dashed lines) and hydrogen bond (green dashed lines) interactions between 14-3-3 $\sigma$ and the isopropyl of FC-THF. ....	20
Figure 2.3	(a) Chemical structure of FC-NAc. (b) 3D complex of 14-3-3 $\sigma$ /TASK-3 with FC-NAc (PDB: 6GHP) revealed hydrophobic (purple dashed lines) and hydrogen bond (green dashed lines) interactions between 14-3-3 $\sigma$ and the 19-acetamide moiety of FC-NAc (dashed circles). ....	21
Figure 2.4	(a) Chemical structure of DP-005. (b) 14-3-3 $\sigma$ /DP-005/p65_45R ternary complex (PDB: 6NV2) showed that DP-005 not only forms hydrophobic interactions (purple dashed lines) with 14-3-3 $\sigma$ , but also with P65_45 (dashed circle). ....	22
Figure 2.5	(a) Chemical structure of fragment-derived small molecule stabilisers of 14-3-3 $\sigma$ PPI. (b) 14-3-3 $\sigma$ /P65/TCF521-123 ternary complex (PDB: 6YPY). (c) 14-3-3 $\sigma$ /P65/TCF521-129 ternary complex (PDB: 6YQ2). ....	23
Figure 2.6	(a) Chemical structure of 28. (b) 14-3-3 $\sigma$ /Pin1/28 ternary complex (PDB: 7BFW). ....	24
Figure 2.7	(a) Chemical structure of fragments 1 and 2. ....	25
Figure 2.8	(a) Chemical structure of AZ003 and AZ008. (b) 14-3-3 $\sigma$ /TAZ/AZ-003 ternary complex (PDB: 6RHC). (c) Docked structure of AZ-008/14-3-3 $\sigma$ in complex with p53pT387. Water-mediated hydrogen bonds are shown as blue dashes, while hydrogen bond and ionic interactions are shown as green and orange dashed lines, respectively. ....	26
Figure 2.9	(a) Chemical structure of 22. (b) 14-3-3 $\sigma$ /Amot-p130/22 ternary complex (PDB: 7NPG). ....	27

Figure 2.10	(a) Chemical structure of Pyrrolidone1. (b) Chemical structure of (R)-Pyrrolidone1. (c) 14-3-3 $\sigma$ /ER $\alpha$ (pT <sup>594</sup> )/Pyrrolidone1 ternary complex (PDB:6TJM).....	28
Figure 2.11	Chemical structure of (S)-Pyrrolidone1, (S)-18, and (-)-28.....	29
Figure 2.12	(a) Chemical structure of phosphonate- and phosphate-type small molecule inhibitors of 14-3-3 $\sigma$ . (b) 14-3-3 $\sigma$ /IMP complex (PDB 6TLF). (c) 14-3-3 $\sigma$ /PLP complex (PDB 6TM7). Hydrogen bond and ionic interactions are shown as green and orange dashed lines, respectively. ....	31
Figure 2.13	(a) Chemical structure of molecular tweezer inhibitor (21). (b) Mode of interaction between Lys residue and molecular tweezer inhibitor, with van der Waals interactions (purple dashed lines), hydrogen bond (green dashed line) and ionic interaction (orange dashed lines). (c) Representation of the 17 surface Lys residues of 14-3-3 $\sigma$ (ball and stick), with molecular tweezer binding at the periphery (square box). ....	32
Figure 2.14	Crystal structure of the MT-ExoS ligand (compound 22) (gray stick) in complex with 14-3-3 $\sigma$ (white surface) (PBD: 6Y7T).....	34
Figure 2.15	Chemical structure of non-phosphonate carboxylate-type small molecule synthetic inhibitor.....	35
Figure 2.16	Chemical structure of non-phosphonate synthetic peptide inhibitors. ....	36
Figure 2.17	Chemical structure of non-phosphonate small molecule inhibitors from natural source. ....	37
Figure 2.18	Chemical structures of GCP-Lys-OMe and Fragment 2.....	42
Figure 3.1	Research flow chart.....	58
Figure 3.2	pEX-N-GST vector. ....	60
Figure 3.3	Chemical structure of fragment 3.....	64
Figure 4.1	The X-ray crystal structure of 14-3-3 $\sigma$ dimer (PDB ID: 1YZ5). Two amphipathic ligand-binding pockets (gray circles) and a	

cavity at the homodimer interface (orange circle) were identified by FTMap as the binding hot spots. Residues lining the amphipathic ligand binding pockets of 14-3-3 $\sigma$  homodimer (white/cyan surface) are labelled, with key interacting residues highlighted in red. The probes (shown in sticks) are mainly bound at the centre cavity of the homodimer interface and the amphipathic pockets (monomer A and monomer B) of 14-3-3 $\sigma$ ..... 80

Figure 4.2	Binding site of fragment 3 on 14-3-3 $\sigma$ (Valenti et al., 2019). ....	81
Figure 4.3	Binding site of fragment 3 (largest cluster) based on the molecular docking results. ....	82
Figure 4.4	Binding modes of top ranked compound (Zinc000082632746) at the dimer interface of 14-3-3 $\sigma$ protein. The conformer with the lowest binding free energy is observed to bind to one site of the 14-3-3 $\sigma$ 's interface cavity, while the conformer from the largest cluster exhibits binding to the opposite site of the putative cavity. ...	83
Figure 4.5	Binding mode of compound I (lowest energy conformation) at the dimer interface of 14-3-3 $\sigma$ protein.....	84
Figure 4.6	Similarity search and molecular docking (VS workflow) in identification of potential small molecule compound targeting the dimer interface of 14-3-3 $\sigma$ . ....	85
Figure 4.7	(A) Blind docking of GCP-Lys-OMe against 14-3-3 $\zeta$ . The protein is represented as red and blue coloured surface for both monomers respectively, while the docked is compound indicated by yellow circle and shown as stick.....	86
Figure 4.8	Focused docking of GCP-Lys-OMe into the dimer interface of 14-3-3 $\zeta$ (A). 2D interaction map resulted from focused docking of GCP-Lys-OMe into the dimer interface of 14-3-3 $\zeta$ (B); docked compound is shown as stick with carbon coloured grey while the dimer interface residues of 14-3-3 $\zeta$ protein are shown as discs and coloured based on their interaction type. ....	87

Figure 4.9	Sequence alignment of the dimer interface helices (H1–H4) of the human 14-3-3 $\sigma$ and human 14-3-3 $\zeta$ isoforms (UniProtKB codes, human 14-3-3 $\sigma$ : P31947; human 14-3-3 $\zeta$ : P63104 as performed with ClustalW and ESPript 3.0, with the red box, white character: strict identity; red character: similarity in the group; blue frame: similarity across the group. ....	88
Figure 4.10	Docking of GCP-Lys-OMe against 14-3-3 $\sigma$ . (A) The protein is represented as the red- and blue-coloured surface for each monomer, respectively, while the docked compound (lowest binding energy conformation, in the stick representation) is indicated by a black box. (B) Two-dimensional (2D) interaction map showing the interactions between GCP-Lys-OMe and the homodimer interface of 14-3-3 $\sigma$ . The docked compound is shown as a stick with gray-coloured carbon while the residues at the homodimer interface of 14-3-3 $\sigma$ protein are shown as discs and coloured based on their types of interaction with the compound. ....	89
Figure 4.11	The RMSD plots of the protein and ligand backbone atoms for the simulated systems of the apo form of 14-3-3 $\sigma$ (PDB: 1YZ5) and the 14-3-3 $\sigma$ /GCP-Lys-OMe complex. ....	90
Figure 4.12	Superimposition of the initial conformation (white ribbon) and 100 ns conformation of the 14-3-3 $\sigma$ protein of the apo system (red ribbon). ....	92
Figure 4.13	Superimposition of the initial conformation (white ribbon) and 100 ns conformation of the 14-3-3 $\sigma$ protein of the 14-3-3 $\sigma$ /GCP-Lys-OMe system (cyan ribbon). The corresponding conformations of the compound GCP-Lys-OMe initially and at 100 ns are shown in white and yellow sticks, respectively. ....	93
Figure 4.14	Snapshots of the simulated 14-3-3 $\sigma$ / GCP-Lys-OMe complex at 0 ns, 20 ns, 40 ns, 60 ns, 80 ns and 100 ns, along with their corresponding 2D interaction maps. ....	94
Figure 4.15	Root-mean-square fluctuation (RMSF) of the C $\alpha$ atoms versus residue number for (A) monomer A and (B) monomer B of 14-3-	



	3 $\sigma$ for the simulated systems of the apo form of 14-3-3 $\sigma$ and the 14-3-3 $\sigma$ /GCP-Lys-OMe complex. Loop regions are indicated by gray shades, while the residues at the homodimer interface are indicated by black arrows. ....	96
Figure 4.16	Plots of the distance between the mass centre of the helices H1 to H4 from both monomers of 14-3-3 $\sigma$ in the apo (black) and GCP-Lys-OMe-bound complex (red). ....	97
Figure 4.17	Changes in the number of contacts between the helices H1 to H4 from both monomers of 14-3-3 $\sigma$ in the apo (black) and GCP-Lys-OMe-bound complex (red).....	98
Figure 4.18	Comparative change in number of intramolecular hydrogen bonds during 100 ns simulation for 14-3-3 $\sigma$ (Apo, black) and GCP-Lys-OMe-bound complex (red).....	99
Figure 4.19	Hydrogen bond profile of the dimer interface residues of the apo 14-3-3 $\sigma$ (A) and 14-3-3 $\sigma$ /GCP-Lys-OMe (B) systems.....	100
Figure 4.20	Projection of motion of protein atoms along the first two dominant eigenvectors (PC1 and PC2) of the apo 14-3-3 $\sigma$ (blue) and 14-3-3 $\sigma$ /GCP-Lys-OMe complex systems (orange).....	104
Figure 4.21	Blind docking result (lowest energy conformation) of the proposed peptides against 14-3-3 $\sigma$ . The protein is represented as red and blue coloured surface for monomers A and B respectively, while the docked peptides are shown as stick.....	107
Figure 4.22	Binding orientation and two-dimensional (2D) interaction maps showing the different interactions between Peptides 3, 5, 9 and 16, and the dimer interface of 14-3-3 $\sigma$ . The docked peptide is shown as stick with carbon atoms coloured gray, while the interacting residues of 14-3-3 $\sigma$ protein are shown as discs and coloured based on their interaction types with the peptides. ....	109
Figure 4.23	The RMSD plots of the protein backbone atoms for the apo 14-3-3 $\sigma$ (black) and 14-3-3 $\sigma$ /Peptide 3 (red) simulated systems, and the	

	backbone atoms of Peptide 3 (relative to the backbone of 14-3-3 $\sigma$ ) in the 14-3-3 $\sigma$ /Peptide 3 simulated system (blue). .....	110
Figure 4.24	Superimposition of the initial conformation (white ribbon) and 100 ns conformation of the 14-3-3 $\sigma$ protein of the 14-3-3 $\sigma$ /Peptide 3 system (cyan ribbon). The corresponding conformations of the Peptide 3 at 0 ns and 100 ns are shown in white and yellow sticks, respectively. ....	112
Figure 4.25	Snapshots of the simulated 14-3-3 $\sigma$ /Peptide 3 complex at 0 ns, 20 ns, 40 ns, 60 ns, 80 ns and 100 ns, along with their corresponding 2D interaction maps. ....	113
Figure 4.26	Root-mean-square fluctuation (RMSF) of the C $\alpha$ atoms versus residue number for monomer A (A) and monomer B (B) of 14-3- 3 $\sigma$ for the simulated systems of the apo form of 14-3-3 $\sigma$ and the 14-3-3 $\sigma$ /Peptide 3 complex during the 100 ns MD simulations. Loop regions are indicated by gray shades, while the residues at the homodimer interface are indicated by black arrows. ....	115
Figure 4.27	Number of contacts between helices H1–H4 of the two monomers of 14-3-3 $\sigma$ during 100 ns MD simulations of 14-3-3 $\sigma$ (apo) (black) and 14-3-3 $\sigma$ /Peptide 3 (red) complex. ....	116
Figure 4.28	Comparative change in number of intramolecular hydrogen bonds during 100 ns simulation for 14-3-3 $\sigma$ (Apo, black) and 14-3- 3 $\sigma$ /Peptide 3 (red).....	117
Figure 4.29	Projection of motion of protein atoms along the first two dominant eigenvectors (PC1 and PC2) of the apo 14-3-3 $\sigma$ (blue) and 14-3- 3 $\sigma$ /Peptide 3 complex systems (orange) based on the 100 ns MD simulations trajectories. ....	119
Figure 4.30	LC chromatogram (top) and mass spectrum (bottom) of Peptide 3. .....	120
Figure 4.31	LC chromatogram (top) and mass spectrum (bottom) of Peptide 5. .....	121

Figure 4.32	LC chromatogram (top) and mass spectrum (bottom) of Peptide 9. .....	121
Figure 4.33	LC chromatogram (top) and mass spectrum (bottom) of Peptide 16.....	122
Figure 4.34	1D <sup>1</sup> H NMR spectrum of Peptide 3. ....	123
Figure 4.35	1D <sup>1</sup> H NMR spectrum of Peptide 5. ....	123
Figure 4.36	1D <sup>1</sup> H NMR spectrum of Peptide 9. ....	124
Figure 4.37	1D <sup>1</sup> H NMR spectrum of Peptide 16. ....	124
Figure 4.38	SDS-PAGE analysis on protein expression of full-length human GST-14-3-3σ in <i>E. coli</i> BL21 (DE3). Lane 1: Soluble fraction after IPTG induction; Lane 2: Insoluble fraction after IPTG induction; Lane 3: Soluble cell lysate without IPTG induction (negative control); Lane 4: Insoluble cell lysate without IPTG induction (negative control), M: standard protein marker. ....	126
Figure 4.39	SDS-PAGE analysis on protein purification of GST-14-3-3σ using GST HiTrap column. Lane 1: Cell lysate (soluble fraction). Lane 2: Flow-through fraction; Lane 3: Wash fraction; Lane 4-8: GST-14-3-3σ elution fractions, M: standard protein marker.....	126
Figure 4.40	(A) SDS-PAGE analysis on protein purification of 14-3-3σ using GST HiTrap and MBP HiTrap columns. Lane 1: Cell lysate (soluble fraction); Lane 2: Cleavage reaction mixture; Lane 3: Flow-through fraction after treatment with GST HiTrap and MBP HiTrap column; Lane 4: Elution fraction collected after treatment with GST HiTrap column. (B) Native PAGE analysis of the purified N-GST-14-3-3σ and 14-3-3σ. ....	127
Figure 4.41	<sup>1</sup> H NMR spectrum of the purified 14-3-3σ protein in 100 mM sodium phosphate, 50 mM NaCl, pH 6.8, at 23 °C.....	128
Figure 4.42	<i>De novo</i> sequencing analysis of the purified 14-3-3σ protein. ....	129
Figure 4.43	1D [ <sup>1</sup> H]-CPMG NMR spectra of 1 mM of Peptides 3, 5, 9 and 16 alone in 100 mM phosphate buffer, 50 mM NaCl, pH 7, 10% <sup>2</sup> H <sub>2</sub> O at 293 K (blue, green, yellow, and dark green, respectively), and in	

	the presence of 50 $\mu\text{M}$ 14-3-3 $\sigma$ (red, black, orange, and magenta respectively) (all peaks are manually shifted 0.02 ppm upfield for clarity). The addition of 14-3-3 $\sigma$ protein to the peptides decreases the signal intensity of all peptides' peaks, except for the peaks at 1.85 ppm and 1.90 ppm (which are likely to be impurity peaks from the buffer).....	130
Figure 4.44	1D [ $^1\text{H}$ ]-CPMG NMR spectra of (A) 1 mM Peptide 3 alone (blue), 1 mM Peptide 3 + 50 $\mu\text{M}$ 14-3-3 $\sigma$ protein (red), and 1 mM Peptide 3 + 50 $\mu\text{M}$ 14-3-3 $\sigma$ protein + 1 mM ExoS (green), and (B) 1 mM ExoS alone (black), 1 mM ExoS + 50 $\mu\text{M}$ 14-3-3 $\sigma$ protein (magenta), and 1 mM ExoS + 50 $\mu\text{M}$ 14-3-3 $\sigma$ protein + 1 mM Peptide 3 (green) in 100 mM phosphate buffer, 50 mM NaCl, pH 7, 10% $^2\text{H}_2\text{O}$ at 293 K. ....	131
Figure 4.45	ITC thermogram of 100 $\mu\text{M}$ 14-3-3 $\sigma$ and 1 mM Peptide 3 in 25 mM HEPES buffer, 100 mM NaCl, pH 7.4 at 298 K. The last three injections showed inconsistent spikes from the first 15 injections and hence they were excluded from the fitting.....	132
Figure 4.46	ITC thermogram of peptide-to-buffer control in 25 mM HEPES buffer, 100 mM NaCl, pH 7.4 at 298 K. ....	133
Figure 4.47	Aggregation point determination using DLS for the 14-3-3 $\sigma$ protein (apo), with volume distribution (red) and intensity distribution (green).....	134
Figure 4.48	Volume distribution profiles of 14-3-3 $\sigma$ protein (apo) at different temperatures. Three independent measurements were taken for each temperature. The particle diameter range for different possible forms of 14-3-3 $\sigma$ are highlighted as follows: 14-3-3 $\sigma$ monomer (orange), homodimer (blue) and aggregates (gray) (Bartsch et al., 2019; Erickson, 2009).....	135
Figure 4.49	Aggregation point determination for the 14-3-3 $\sigma$ protein in the presence of Peptide 3 with volume distribution (red) and intensity distribution (green).....	136

Figure 5.1 An example of  $^1\text{H}$  NMR spectrum of an unfolded protein. No peak was observed below 0.8 ppm (red circle) with a dominant peak at approximately 1 ppm (black arrow) in the aliphatic region, while the peaks downfield of 8.5 ppm in the amide region are broad and less dispersed (blue circle). Adapted from Rehm et al., 2002. .... 150

## LIST OF SYMBOLS

%	Percentage
°C	Degree Celsius
Å	Angstrom
h	Hour
mL	Millilitre
nm	Nanometer
ppm	Parts per Million
rpm	Revolution per Minute
v/v	Volume/Volume
μL	Microliter
μM	Micromolar

## LIST OF ABBREVIATIONS

1D	One-Dimensional
AMBER	Assisted Model Building with Energy Refinement
CADD	Computer-Aided Drug Design
CHARMM	Chemistry At Harvard Macromolecular Mechanics
CPMG	Carr-Purcell-Meiboom-Gill
DEAE	Diethylaminoethyl
DIPEA	N,N-Diisopropylethylamine
DLS	Dynamic Light Scattering
DMB	1,3-Dimethoxybenzene
DMF	Dimethylformamide
DS	Discovery Studio
EDT	1,2-Ethanedithiol
FP	Fluorescence Polarisation
GCP	Guanidiniocarbonyl Pyrrole
GROMACS	Groningen Machine for Chemical Simulations
GST	Glutathione S-Transferases
HCTU	O-(1h-6-Chlorobenzotriazole-1-Yl)-1,1,3,3-Tetramethyluronium Hexafluorophosphate
HEPES	4-(2-Hydroxyethyl)-1-Piperazineethanesulfonic Acid
HPLC	High Performance Liquid Chromatography
IPTG	Isopropyl $\beta$ -D-1-thio-galactopyranoside
ITC	Isothermal Titration Calorimetry
$K_D$	Binding Affinity
LB	Luria Broth
LC-MS	Liquid Chromatography-Mass Spectroscopy
MD	Molecular Dynamics
MS	Mass Spectrometry
MST	Microscale Thermophoresis
NAMD	Nanoscale Molecular Dynamics
NMR	Nuclear Magnetic Resonance
NPT	Constant Number of Particle (N), Pressure (P) and Temperature (T)

NVT	Constant Number of Particle (N), Volume (V) and Temperature (T)
OPLS	Optimized Potential for Liquid Simulations
PCA	Principal Component Analysis
PDB	Protein Data Bank
PME	Particle Mesh Ewald
PPI	Protein–Protein Interaction
QM/MM	Quantum Mechanics/Molecular Mechanics
RMSD	Root-Mean-Square Deviation
RMSF	Root-Mean-Square Fluctuation
RP-HPLC	Reverse-Phase High-Performance Liquid Chromatography
SDS	Sodium Dodecyl Sulfate
PAGE	Polyacrylamide Gel Electrophoresis
SPPS	Solid Phase Peptide Synthesis
TFA	Trifluoroacetic Acid
TIPS	Triisopropylsilane
TN	Tris-NaCl
UFLC	Ultra-Fast Liquid Chromatography
UHPLC	Ultra-High-Performance Liquid Chromatography
vdW	van der Waals
VS	Virtual Screening
WHO	World Health Organisation



# PENGENALPASTIAN PENSTABIL HOMODIMER 14-3-3 SIGMA BAHARU DALAM KARSINOMA NASOFARINKS

## ABSTRAK

14-3-3 $\sigma$  ialah protein homodimer berasid dengan lebih daripada seratus pasangan protein yang berbeza yang berkaitan dengan pengisyaratan onkogenik dan pengawalaturan kitaran sel. Kajian terdahulu menunjukkan bahawa 14-3-3 $\sigma$  berfungsi sebagai penindas tumor yang berpotensi dan ekspresinya biasa diturunkan dalam banyak jenis kanser termasuk karsinoma nasofarinks (NPC). Selain itu, oleh sebab 14-3-3 $\sigma$  perlu membentuk homodimer untuk berfungsi secara aktif, penstabil homodimer dijangka juga dapat meningkatkan aktiviti 14-3-3 $\sigma$ . Namun demikian, sehingga kini masih tidak ada ligan yang dilaporkan dapat mengikat pada rongga antara muka dimer 14-3-3 $\sigma$  dan menstabilkan bentuk homodimerinya. Oleh itu, tujuan kajian ini adalah untuk mengenal pasti penstabil homodimer 14-3-3 $\sigma$  baharu yang berpotensi. Tiga pendekatan berbeza telah dilaksanakan untuk mengenal pasti penstabil homodimer 14-3-3 $\sigma$  baharu yang berpotensi, iaitu penyaringan maya *in silico* terhadap pangkalan data komersial sedia ada, mencari dalam literatur untuk sebatian yang dilaporkan menyasarkan antara muka dimer isoform 14-3-3 yang lain, dan reka bentuk rasional penstabil homodimer 14-3-3 $\sigma$  baharu yang berpotensi. Pendokkan molekul *in silico* dan simulasi dinamik molekul (MD) dengan pelbagai alat analisis (telah dilaksanakan untuk mengenal pasti penstabil homodimer 14-3-3 $\sigma$  baharu yang berpotensi. Peptida yang direka dengan rasional dan menunjukkan tenaga bebas ikatan yang lebih rendah pada 14-3-3 $\sigma$  telah disintesis dengan menggunakan pendekatan sintesis peptida fasa pepejal (SPPS) dan dicirikan menggunakan  $^1\text{H}$  NMR dan LC-MS. Di samping itu, protein 14-3-3 $\sigma$  manusia yang lengkap telah diekspresikan dan dicirikan menggunakan

SDS-PAGE, PAGE asli,  $^1\text{H}$  NMR, dan analisis penjujukan. Kajian pengikatan peptida yang disintesis pada protein 14-3-3 $\sigma$  yang diekspresikan secara rekombinan dengan menggunakan  $[\text{H}^1]$ -Carr-Purcell-Meiboom-Gill (CPMG) NMR mengesahkan pengikatan peptida pada protein 14-3-3 $\sigma$ . Walau bagaimanapun, analisis kalorimetri pentitratan isoterma (ITC) menunjukkan keafinan ikatan yang agak lemah oleh sebatian terbaik (Peptida 3) daripada kajian pendokkan molekul pada protein 14-3-3 $\sigma$ . Namun demikian, analisis penyerakan cahaya dinamik (DLS) menunjukkan bahawa protein 14-3-3 $\sigma$  hanya mula membentuk agregat pada 48 °C dengan kehadiran Peptida 3, berbanding dengan 43 °C tanpa Peptida 3. Oleh sebab analisis DLS pada protein sahaja pada suhu terpilih (25, 42, 50, dan 60 °C) jelas menunjukkan bahawa bentuk homodimer protein tersebut berpecah kepada monomer sebelum pengagregatan lengkap, keputusan ini menunjukkan bahawa Peptida 3 mampu menstabilkan bentuk homodimer protein 14-3-3 $\sigma$  daripada berpecah menjadi monomer, dan seterusnya menyokong peranan Peptida 3 sebagai penstabil homodimer 14-3-3 $\sigma$  yang berpotensi. Kesimpulannya, kajian ini telah berjaya mengenal pasti penstabil homodimer 14-3-3 $\sigma$  yang baharu. Walaupun keafinan ikatan Peptida 3 tidak sekuat seperti yang dijangkakan *in silico*, kajian ini telah membuktikan keupayaan berpotensi suatu sebatian dengan dua kumpulan berfungsi asas yang dipisahkan oleh jarak tertentu (13 atom karbon) untuk mengikat dan menstabilkan bentuk homodimer 14-3-3 $\sigma$  yang penting untuk fungsi penindasan tumornya.

# IDENTIFICATION OF NOVEL 14-3-3 SIGMA HOMODIMER STABILISER IN NASOPHARYNGEAL CARCINOMA

## ABSTRACT

14-3-3 $\sigma$  is an acidic homodimer protein with more than one hundred different protein partners associated with oncogenic signalling and cell cycle regulation. Previous studies have shown that 14-3-3 $\sigma$  functions as a potential tumour suppressor and its expression is commonly downregulated in many types of cancer including nasopharyngeal carcinoma (NPC). As the monomers are generally more prone to degradation than dimers, it was hypothesised that a homodimer stabiliser can potentially decrease the degradation of 14-3-3 $\sigma$ . Also, as the 14-3-3 $\sigma$  requires homodimer form to be functionally active, a homodimer stabiliser is expected to also enhance the activity of the 14-3-3 $\sigma$ . However, to date, there is no reported ligand that can bind to the 14-3-3 $\sigma$  dimer interface cavity and stabilise its homodimeric form. Thus, the aim of this study is to identify a potential novel 14-3-3 $\sigma$  homodimer stabiliser. Three different approaches were implemented to identify a potential novel 14-3-3 $\sigma$  homodimer stabiliser, i.e., *in silico* virtual screening of a commercially available database, searching the literature for compounds reported to target the dimer interface of other 14-3-3 isoforms, and rational design of potentially novel 14-3-3 $\sigma$  homodimer stabilisers. *In silico* molecular docking and molecular dynamic (MD) simulation with various analysis tools were implemented for the identification of the potential 14-3-3 $\sigma$  homodimer stabiliser. The rationally designed peptides, which showed lower binding free energy to the 14-3-3 $\sigma$ , were synthesised, using solid phase peptide synthesis approach (SPPS), and characterised using  $^1\text{H}$  NMR and LC-MS. On the other hand, the full-length human 14-3-3 $\sigma$  protein was expressed and further characterised using

SDS-PAGE, native PAGE,  $^1\text{H}$  NMR, and sequencing analysis. Subsequent binding study of the synthesised peptides to the recombinantly expressed 14-3-3 $\sigma$  protein using [ $^1\text{H}$ ]-Carr-Purcell-Meiboom-Gill (CPMG) NMR confirmed the binding of the peptides to the 14-3-3 $\sigma$  protein. Isothermal titration calorimetry (ITC) analysis, however, indicated a relatively weak binding affinity of the top ranked compound (Peptide 3) from the molecular docking studies on the 14-3-3 $\sigma$ . Nevertheless, dynamic light scattering (DLS) analysis revealed that the 14-3-3 $\sigma$  protein only started to aggregate at 48 °C in the presence of Peptide 3, compared to 43 °C in the absence of Peptide 3. As the DLS analysis of the protein alone at selected temperature (25, 42, 50, and 60 °C) clearly showed that the protein's homodimer form dissociated into monomer before complete aggregation, these results seem to indicate that Peptide 3 is able to stabilise the homodimer form of 14-3-3 $\sigma$  protein from dissociating into monomers, thus supporting its role as a potential 14-3-3 $\sigma$  homodimer stabiliser. In conclusion, this study has successfully identified a novel 14-3-3 $\sigma$  homodimer stabiliser. Although the binding affinity of the Peptide 3 was not as good as predicted *in silico*, this study has demonstrated the potential ability of a compound with two basic functional groups separated by a specific distance (13 carbon atom) to bind and stabilise the 14-3-3 $\sigma$  homodimer form which is essential for its tumour suppressing functions.

# CHAPTER 1

## INTRODUCTION

### 1.1 Background of the study

#### 1.1.1 Nasopharyngeal carcinoma (NPC)

NPC is a type of head and neck cancer that develops in the epithelial lining of the nasopharynx, commonly originated in the fossa of Rosenmuller, a recess located medial to the medial crura of the Eustachian tube (Chen et al., 2019). NPC is characterised by Epstein–Barr virus (EBV) infection, hidden anatomical location, remarkable racial and geographical distribution, and high incidence of locoregional recurrence or metastasis (Xiao et al., 2009). According to the International Agency for Research on Cancer, NPC is considered a rare malignancy accounting for only 0.7 % of all cancers diagnosed in 2020 with an incidence rate of around 1 in every 100,000 persons. Nevertheless, NPC is mostly common in eastern and Southeast Asia (Sung et al., 2021; Chen et al., 2019; World Health Organization, 2020). In Malaysia, NPC is the fourth most common malignant tumour. It is common among the Chinese, followed by natives of Borneo (especially the Bidayuh) and the Malay (Loh et al., 2023).

The aetiology of NPC is related to a combination of a genetic, ethnicity, viral infection, and environmental factors (Chang et al., 2021; Cho, 2007). According to the World Health Organization (WHO), NPCs are classified into three pathological subtypes: keratinising squamous, non-keratinising, and basaloid squamous. The non-keratinising NPC can be also divided into differentiated and undifferentiated tumours. The non-keratinising subtype is considered the most common subtype in the endemic areas and is predominantly associated with Epstein-Barr virus (EBV) infection (Chua et al., 2016; Thompson, 2007; Wang et al., 2016a). Current treatment modality of NPC

is radiotherapy and chemotherapy; however, locoregional recurrence and distant metastases are usually considered the causes of treatment failure (Cao et al., 2013; Chua et al., 2003; Li et al., 2014; Wei and Sham, 2005; Xiao et al., 2009). This suggests the need of a new therapeutic agents against NPC.

### **1.1.2 14-3-3 $\sigma$ (Stratifin, or Sfn)**

The 14-3-3 protein family (tyrosine 3-monooxygenase/tryptophan 5-monooxygenase activation protein) is a group of acidic polypeptides that are highly conserved in all eukaryotic cells (Leffers et al., 1993; Wang and Shakes, 1996; Prasad et al., 1992). The 14-3-3 protein family was initially described by Moore & Perez in 1967 as an abundant mammalian brain proteins found in vertebrates (Moore and Perez, 1967). 14-3-3 proteins have also been detected in non-vertebrate species such as plants and yeasts (Rosenquist et al., 2001; van Heusden, 2009; van Heusden and Steensma, 2006). The family took its name based on its elution profile, specifically the fraction number of bovine brain homogenate from diethylaminoethyl (DEAE) cellulose column (14<sup>th</sup> fraction) and subsequent purified fraction 3.3 from gel electrophoresis (Moore and Perez, 1967). The 14-3-3 proteins were initially considered as activators of enzymes in dopamine and neurotransmitter biosynthesis (Ichimura et al., 1988) before its key role in regulating the activity of the protein kinase C and acting as a substrate for c-Bcr serine/threonine kinases were investigated (Reuther et al., 1994). Later, 14-3-3 proteins were shown to interact with many protein kinases such as Raf (Freed et al., 1994).

The 14-3-3 family comprises of seven human isoforms which are encoded by separate genes (YWHAB, YWHAE, YWHAG, YWHAH, YWHAS/SFN, YWHAQ, YWHAZ) located on different chromosomes. The seven isoforms are named after their respective elution positions on high performance liquid chromatography (HPLC) ( $\beta$ -

beta,  $\epsilon$ -epsilon,  $\gamma$ -gamma,  $\eta$ -eta,  $\sigma$ -sigma,  $\tau$ -tau, and  $\zeta$ -zeta) with more than 1,200 partners forming protein–protein interaction (PPI) in mammalian cells (Sluchanko and Bustos, 2019; Aitken, 2002; Ichimura et al., 1988).

Members of 14-3-3 proteins family share a high degree of sequence similarity (Figure 1.1) with a molecular mass of approximately 28–30 kDa and isoelectric point of 4–5 (Aitken et al., 2002; Fu et al., 2000). In addition, the phylogenetic tree analysis based on the primary sequence of the seven human 14-3-3 isoforms indicates more similarities between certain pairs of 14-3-3 isoforms such as  $\eta$  and  $\gamma$ ,  $\beta$  and  $\zeta$ , as well as  $\sigma$  and  $\tau$  (Figure 1.2).

The 14-3-3 $\sigma$  protein was first identified in differentiated squamous epithelium by Leffers et al. (1993). 14-3-3 $\sigma$  is unique as it is abundantly expressed in the keratinocytes and epithelial cells (Leffers et al., 1993; Prasad et al., 1992). 14-3-3 $\sigma$  regulates a wide range of proteins which are mostly involved in oncogenic signalling and cell cycle regulation (Huang et al., 2020).

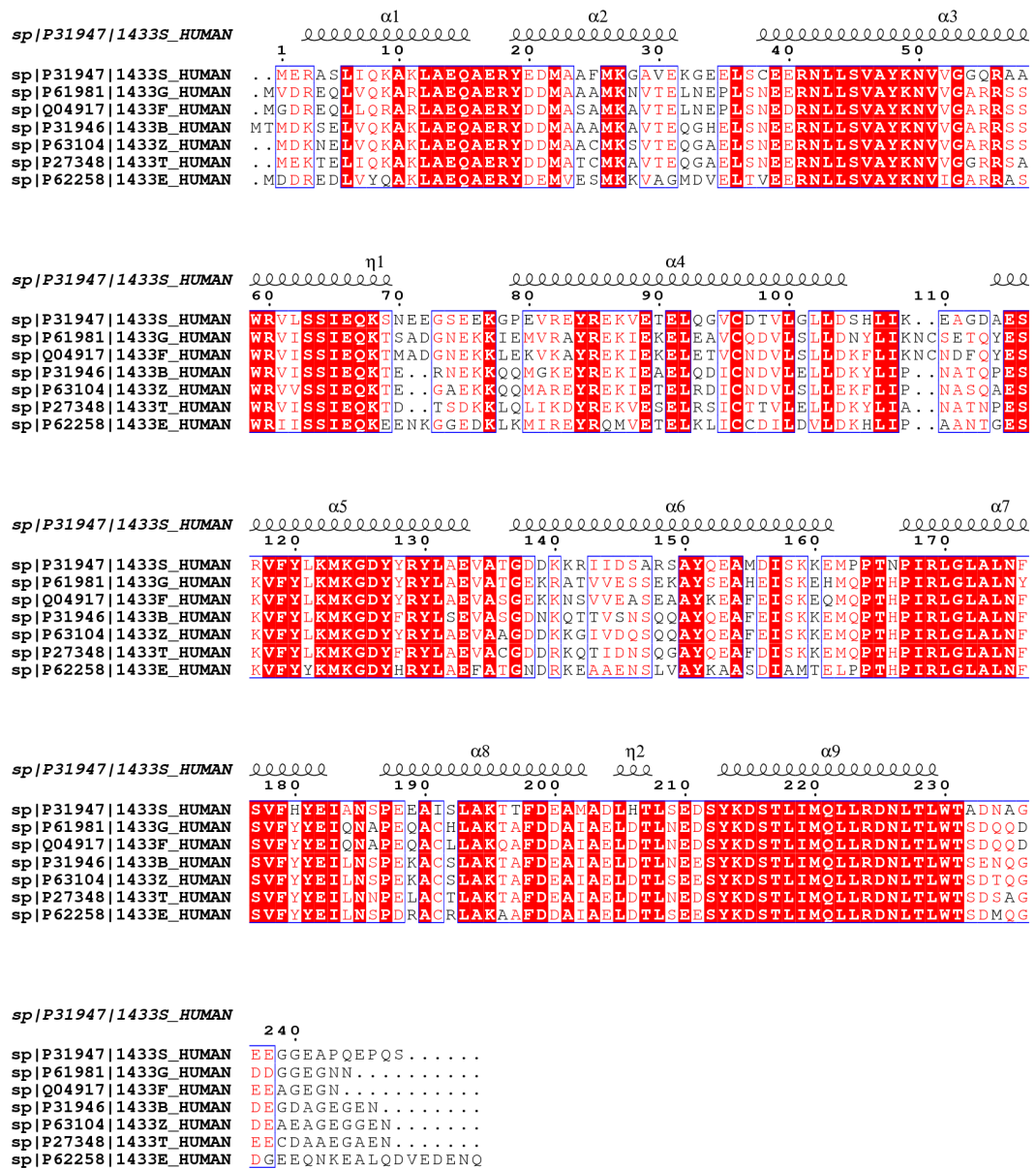


Figure 1.1 Sequence alignment of the seven human 14-3-3 isoforms (UniProtKB codes, h14-3-3ε: P62258; h14-3-3σ: P31947; h14-3-3γ: P61981; h14-3-3η: Q04917; h14-3-3τ: P27348; h14-3-3ζ: P63104; h14-3-3β: P31946), as performed with ClustalW and ESPrnt 3.0, with red box, white character: strict identity; red character: similarity in group; blue frame: similarity across group. The α-helical regions are indicated above the sequence.

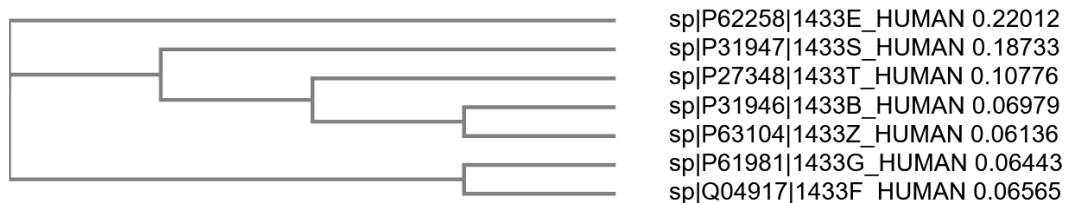


Figure 1.2 Phylogenetic tree of the seven human 14-3-3 isoforms generated using ClustalOmega.



### 1.1.3 Structure of 14-3-3 $\sigma$

Crystal structures of 14-3-3 proteins revealed that they are highly helical dimers with a clamp-like or horseshoe conformation (Figure 1.3). 14-3-3 isoforms can form homo- or heterodimers with other isoforms in which the dimer form of 14-3-3 proteins has two amphipathic binding grooves and thus is capable of binding two ligand motifs at the same time, either from the same target or from two different partners (Yang et al., 2006b; Xiao et al., 1995; Gardino et al., 2006). The amino acids residues lining the amphipathic grooves of the 14-3-3 proteins are highly conserved (Figure 1.4, yellow colour) whereas more variations can be seen on the outer surface.

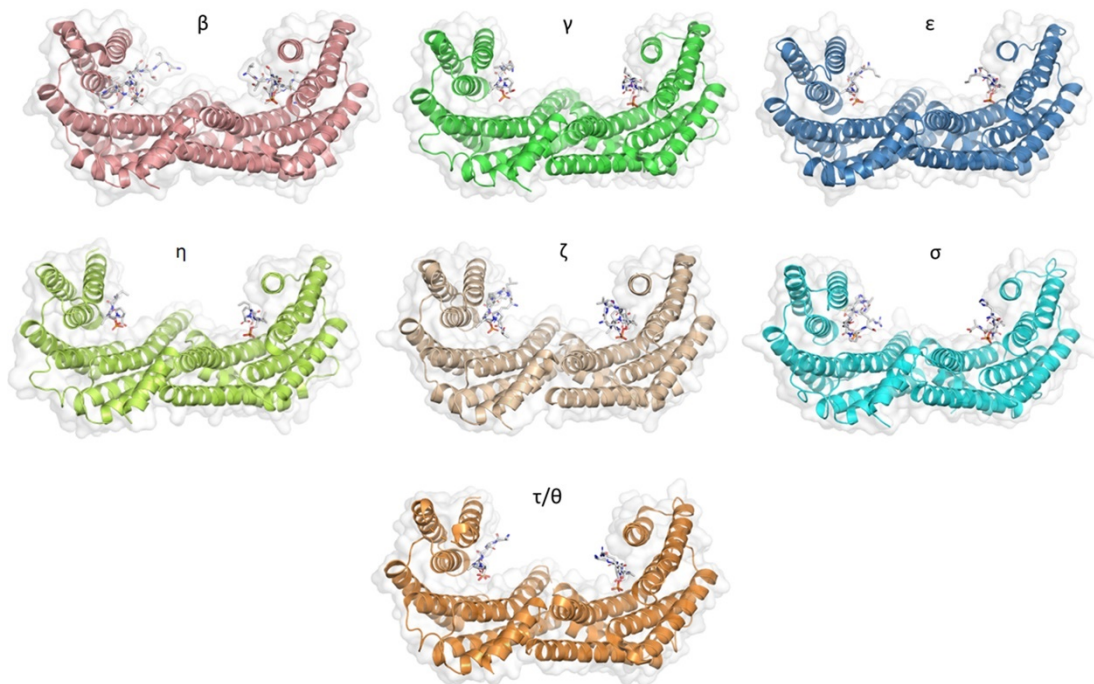


Figure 1.3 Crystal structures of the seven human 14-3-3 isoforms (PDB codes, h14-3-3 $\beta$ : 6A5Q; h14-3-3 $\gamma$ : 2B05; h14-3-3 $\epsilon$ : 2BR9; h14-3-3 $\eta$ : 2C63; h14-3-3 $\zeta$ : 1QJA; h14-3-3 $\sigma$ : 1YWT; h14-3-3 $\tau$ : 2BTP) (presented as ribbon) with their peptide ligands (presented as stick, backbone colour white) bound to the amphipathic binding groove of both monomers.

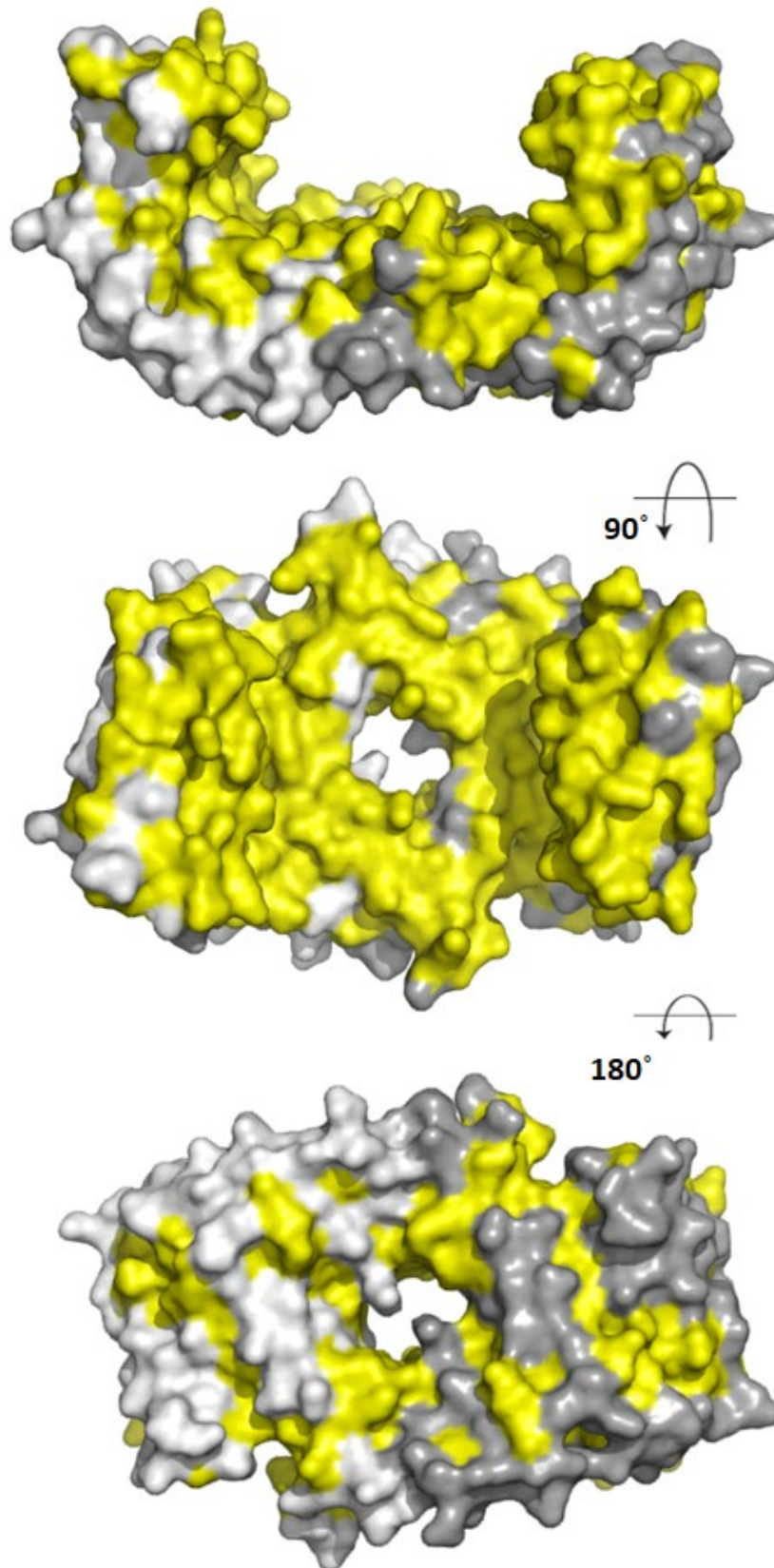


Figure 1.4 Surface representations of the 14-3-3 $\sigma$  homodimer (PDB: 1YWT). The conserved residues are highlighted in yellow colour. The second and third structures are rotated 90° and 180°, respectively, around the x-axis from the previous structure.

Despite the dimeric structural similarity among the mammalian 14-3-3 isoforms, many reports have shown isoform-specific interactions with 14-3-3 binding partners (Aitken et al., 2002; Aitken, 2006; Benzinger et al., 2005). It is believed that the difference in the residues of the region adjacent to the amphipathic groove and the unconserved residues forming the outer surface of 14-3-3 proteins play a key role in 14-3-3 specific binding targets (Gardino et al., 2006; Benzinger et al., 2005). In addition, reports have indicated that the N-terminal as well as the position and angles between the monomers vary among 14-3-3 isoforms, which confer an isoform-specific partner interaction (Benzinger et al., 2005; Yang et al., 2006b).

The 14-3-3 proteins are also classified as phosphoserine/phosphothreonine (pSer/pThr)-recognition proteins, as they generally exert their activity through binding to the phosphoserine/phosphothreonine-containing motifs of a multitude of molecules with various functions such as kinases, phosphatases, transmembrane receptors, and transcription factors (Chen et al., 2018; Lalle and Fiorillo, 2019; Cotellet and Leonhardt, 2016; Fan et al., 2019). In general, there are two high-affinity phosphorylation-dependent binding motifs that are recognised by the amphipathic binding grooves of all 14-3-3 isoforms, i.e., Arg-Ser-Xaa-pSer-Xaa-Pro (R-S-X-pS-X-P, mode I, Figure 1.5a) and Arg-Xaa-Xaa-Xaa-pSer/Thr-Xaa-Pro (R-X-X-X-pS/T-X-P, mode II, Figure 1.5b), where X is any amino acid and pS/T represents phosphorylated serine or threonine (Yaffe et al., 1997). A third binding motif recognised by the C-terminus of 14-3-3 proteins, i.e., pS/pT-X<sub>1-2</sub>-COOH (mode III, Figure 1.5c) has also been reported (Coblitz et al., 2005). Nevertheless, not all 14-3-3 interactions require a phosphorylated residue as 14-3-3 has also been reported to bind to several non-phosphorylated proteins and peptides, such as exoenzyme S, Cdc25B,

and p190RhoGEF (Petosa et al., 1998; Masters et al., 1999; Henriksson et al., 2000; Mils et al., 2000; Zhai et al., 2001; Xu et al., 2019).

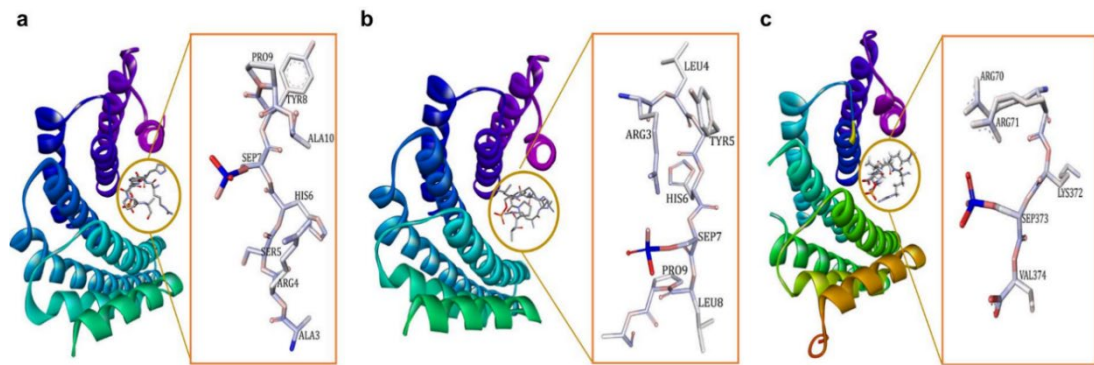


Figure 1.5 (a) 14-3-3 $\zeta$ /phosphopeptide complex (mode I, PDB: 1QJB), (b) 14-3-3 $\zeta$ /phosphopeptide complex (mode II, PDB: 1QJA), (c) 14-3-3 $\sigma$ /TASK3 peptide (mode III, PDB: 6GHP).

The 14-3-3 $\sigma$  isoform only exists as a homodimer because the heterodimer form is destabilised by the force of electrostatic interaction between the residue of Glu in position 80 and the residue of Asp or Glu, that replace Ser in position 5 in the 14-3-3 $\sigma$  structure (Benzinger et al., 2005; Hsu et al., 2018). Like other isoforms, the dimer molecule of 14-3-3 $\sigma$  forms a cup-like shape in which each monomer consists of nine elongated bundles of anti-parallel helices (H1–H9). While four helices (H1–H4) involve in the dimerisation with the other monomer, the remaining five helices (H5–H9) form the amphipathic ligand-binding groove (Figure 1.6) (Benzinger et al., 2005). Earlier reports indicated that the 14-3-3 $\sigma$  protein can be found in either open (apo form) or closed state when it is bound to its target protein or peptides (Hu et al., 2014). While helices H1–H4 were stable in both open and closed state, the intermolecular interactions between the residues in helices H5–H9 were different in the apo-form compared to the bound one. Four hydrophilic residues (Lys49, Arg56, Arg129, and Tyr130) at H3 and H5 have been proposed to contribute to the equilibrium between both states. These residues are believed to form hydrogen bonds with the binding

peptide and drive the transition from the open conformation to the closed conformation (Hu et al., 2014).

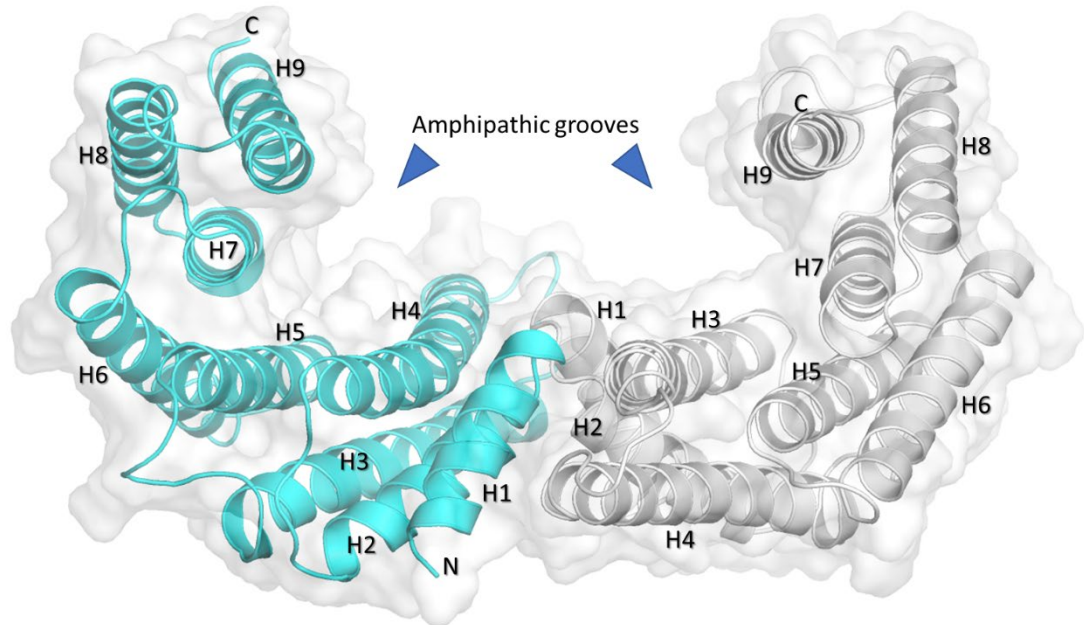


Figure 1.6 Surface representations of the 14-3-3 $\sigma$  homodimer (PDB: 1YZ5). The amphipathic binding grooves are indicated by blue triangles.

Five major non-conserved amino acid residues (Ser5, Glu20, Phe25, Gln55, and Glu80) are located at the interface between both monomers near the N-terminus of the 14-3-3 $\sigma$  isoform. Among them, the residues Ser5, Glu20, Phe25, and Glu80 together with the highly conserved hydrophobic core residues located at the dimer interface, i.e., Leu12 and Tyr84, were found to play a crucial role in the stabilisation of the homodimer molecule and maintaining the full dimerisation activity of 14-3-3 $\sigma$  (Benzinger et al., 2005; Li et al., 2013). This is evidenced by the dissociation of the dimeric 14-3-3 $\sigma$  into monomers with diminished function upon mutation of these residues (Benzinger et al., 2005; Li et al., 2013; Liu et al., 2011).

#### 1.1.4 Role of 14-3-3 $\sigma$ in cancer

Previous studies have demonstrated the role of 14-3-3 $\sigma$  in suppressing tumour metabolic reprogramming (Phan et al., 2015; Wen et al., 2013; Khorrami et al., 2017;

Ji et al., 2018). In addition, a few reports have also highlighted the crucial role of 14-3-3 $\sigma$  against the cancer cell invasion and metastasis. For instance, a low level of 14-3-3 $\sigma$  has been shown to promote production of lactate which stimulates the migration of epithelial cancer cells to a distant organ through breaking down of extracellular matrices (Gatenby and Gillies, 2004; Phan et al., 2015). Studies have also showed that, among all seven well-known human 14-3-3 isoforms, 14-3-3 $\sigma$  is the only isoform that possesses tumour-suppressing activity (Ferguson et al., 2000; Fu et al., 2000; Lee and Lozano, 2006; Hermeking et al., 1997). It has been shown that 14-3-3 $\sigma$  protein directly controls the G2-M checkpoint of the cell cycle by protecting the tumour suppressor factor P53 against the MDM2-mediated ubiquitination and degradation (Yang et al., 2006a; Hermeking et al., 1997). In addition, 14-3-3 $\sigma$  was also reported to play a crucial role in the cell cycle arrest regulation by acting as a cyclin-dependent kinase (Cdk) inhibitor, i.e., through sequestering the cyclin-dependent kinase 1-cyclin B1 complex from entering the nucleus and initiating mitosis, as well as binding to the cyclin-dependent kinases 2 and 4 (Chan et al., 1999; Laronga et al., 2000). Moreover, 14-3-3 $\sigma$  was also found to negatively regulate the oncogenic activity of the Protein kinase B (also known as Akt) and thus protecting against Akt-mediated tumorigenesis (Yang et al., 2006a). Further, 14-3-3 $\sigma$  has also been reported as a target gene in mammary epithelial cells which regulates the antiproliferative activity of the transforming growth factor-beta 1 (TGF- $\beta$ 1) through the Smad3-dependent mechanism (Hong et al., 2010; Hong et al., 2013). Furthermore, reports have demonstrated 14-3-3 $\sigma$  involvement in controlling cell proliferation and cancer metastasis via the termination of NF- $\kappa$ B signal in mammary cells by regulating the nuclear export of the p65 subunit of NF- $\kappa$ B transcription factor and subsequently inhibits its transcriptional activity (Ingles-Esteve et al., 2012; Wolter et al., 2020). Moreover, 14-3-3 $\sigma$  has also been reported to regulate



the expression of human TASK-3 channel (which is believed to facilitate cancer cell proliferation and survival), by blocking the endoplasmic reticulum retention sequences, and thereby promoting the surface expression of this channel (Aghazadeh and Papadopoulos, 2016; Anders et al., 2013; Zúñiga et al., 2018). 14-3-3 $\sigma$  also regulates the oncogenic activity of transcriptional coactivator TAZ which is an oncogenic protein that promotes cell proliferation and migration. The binding of TAZ to 14-3-3 $\sigma$  leads to cytoplasmic retention of TAZ which subsequently disabling its function (Zhou and Lei, 2016).

Although some studies have also indicated that the 14-3-3 $\sigma$  could be a double-edged sword (Li et al., 2009), whereby its upregulation has been linked with resistance to chemotherapeutic agents (Han et al., 2006; Liu et al., 2006; Zhang and Liu, 2007), overexpression of matrix metalloproteinase 1 (MMP-1), a proteolytic enzyme that degrades native fibrillar collagens, poor prognosis in malignant tumours, including gastric and colon carcinomas (Ghahary et al., 2005; Li et al., 2009; Murray et al., 1996; Inoue et al., 1999), and to binding to the c-Abl protein in chronic myeloid leukaemia, preventing its nuclear translocation and subsequently interfering with its pro-apoptotic effect (Mancini et al., 2009), the vital role of 14-3-3 $\sigma$  in controlling the tumour formations and metastasis in NPC has been fairly consistent (Chen et al., 2015; Huang et al., 2010; Xie et al., 2019).

### **1.1.5 Expression of 14-3-3 $\sigma$ in NPC**

Unlike other isoforms which show elevated expression in many types of cancer, 14-3-3 $\sigma$  protein level is downregulated in chronic myeloid leukaemia, nasopharyngeal carcinoma, as well as lung, breast, oesophageal, uterine, ovarian, and skin cancers (Chan et al., 2010; Fan et al., 2019; Li et al., 2009; Lodygin et al., 2003;

Qi et al., 2014; Zhou et al., 2018). The low expression level of 14-3-3 $\sigma$  protein in many cancer types has been linked to either promoter hypermethylation of Sfn gene (which encodes the 14-3-3 $\sigma$  protein) or direct 14-3-3 $\sigma$  degradation through ubiquitination which eventually aborts the normal physiological role of 14-3-3 $\sigma$  against tumour growth and metastasis (Choi et al., 2011; Ferguson et al., 2000; Umbrecht et al., 2001; Urano et al., 2002; Vercoutter-Edouart et al., 2001). Previous research has identified TRIM25 (EFP), RFFL (CARP2), COPS5, and LASP1 as potential partners that could facilitate the degradation of 14-3-3 $\sigma$  protein. (Urano et al., 2002; Yang et al., 2008; Zhou et al., 2018). EFP is a member of the RING-finger B-box coiled-coil (RBCC) motif family. It is an E3 ubiquitin ligase enzyme that has a RING domain located at the N-terminus that is important for its ubiquitination activity while the C-terminus contains the PRY-SPRY domain which has been proposed to be involved in protein–protein interactions (Martín-Vicente et al., 2017; Sanchez et al., 2016). EFP has been shown to be involved in the regulation of 14-3-3 $\sigma$  in breast cancer by Efp-mediated proteolysis (Urano et al., 2002). The direct degradation of 14-3-3 $\sigma$  by EFP caused the dissociation of the protein from cyclin–Cdk complexes, leading to cell cycle progression and tumour growth (Urano et al., 2002). CARP2 is another E3 ligases that has been found to target 14-3-3 $\sigma$  for degradation in HCT116 and HeLa cells, leading to the stabilisation of MDM2, the major negative regulator of tumour suppressor p53 (Yang et al., 2008). LIM and SH3 protein 1 (LASP1) is a specific focal adhesion protein that is known to be involved in numerous biological and pathological processes (Shao et al., 2016). Upregulation of LASP1 has been found in several types of cancer. It has been reported that LASP1 interacted with 14-3-3 $\sigma$  and negatively regulated the expression of 14-3-3 $\sigma$  in colorectal cancer which results in the progression of the tumour (Zhou et al., 2018). Further analysis showed that COPS5 could directly bind



to the SH3 domain of LASP1, and negatively regulate the expression of 14-3-3 $\sigma$  through ubiquitination and protein degradation thus promoting colorectal cancer progression via PI3K/Akt dependent signalling pathway (Zhou et al., 2018; Shao et al., 2016). While the protein partners involved in degradation of 14-3-3 $\sigma$  in various cancer cell types have been reported, it is still unknown whether the same proteins are involved in the degradation of 14-3-3 $\sigma$  in NPC. However, previous iTRAQ-based quantitative proteomic analysis of CNE1 and CNE2 NPC cell lines has identified TRIM25 and LASP1 proteins (Huang et al., 2010), which suggests their possible involvement in 14-3-3 $\sigma$  degradation in NPC.

## 1.2 Problem Statement

Although many proteins have been reported to be responsible for 14-3-3 $\sigma$  degradation and ubiquitination in various cancer cell types, i.e., TRIM25 (EFP), RFFL (CARP2), COPS5 and LASP1 (Urano et al., 2002; Yang et al., 2008; Zhou et al., 2018), the interaction site of these protein partners on 14-3-3 $\sigma$  and their degradation mechanism, i.e., whether it involves dissociation of 14-3-3 $\sigma$  dimer into monomer, have yet to be determined. Nevertheless, as the monomers are generally more prone to degradation than dimers (Messaritou et al., 2010; Sluchanko et al., 2011), it was hypothesised that a homodimer stabiliser can potentially decrease the degradation of 14-3-3 $\sigma$ . Also, as the 14-3-3 $\sigma$  requires homodimer form to be functionally active, a homodimer stabiliser is expected to also enhance the activity of the 14-3-3 $\sigma$ . Unfortunately, to date, the only modulators of 14-3-3 $\sigma$  are stabilisers and inhibitors of PPI between 14-3-3 $\sigma$  and protein partners at the amphipathic ligand-binding groove, while compounds that were reported to bind at the dimer interface are only for the dimer of 14-3-3 $\zeta$  and 14-3-3 $\eta$  isoforms which have distinctively different dimer interface than 14-3-3 $\sigma$ .

### 1.3 Objectives

The main objective of this study is to identify a novel homodimer stabiliser for 14-3-3 $\sigma$  in NPC. The specific objectives of this study are:

- a) To design and predict potential 14-3-3 $\sigma$  homodimer stabilisers *in silico*.
- b) To synthesise, purify, and characterise selected potential 14-3-3 $\sigma$  homodimer stabilisers designed and predicted from *in silico* study.
- c) To recombinantly express, purify, and characterise the 14-3-3 $\sigma$  protein.
- d) To analyse the interaction between the synthesised potential 14-3-3 $\sigma$  homodimer stabilisers and the recombinantly expressed 14-3-3 $\sigma$  *in vitro*.
- e) To investigate the stabilisation effect of the identified novel 14-3-3 $\sigma$  homodimer stabiliser on 14-3-3 $\sigma$  protein aggregation *in vitro*.

### 1.4 Scope of the thesis

The 14-3-3 $\sigma$  has gain the attention of many researchers as a potential therapeutic target against cancer growth and metastasis. It regulates a wide array of proteins, many of which are involved in oncogenic signalling and the regulation of the cell cycle. While it is known that the homodimer form of 14-3-3 $\sigma$  is essential for its full activity, and that monomers are more prone to degradation than dimers, there are currently no identified ligands that specifically target the central cavity of the 14-3-3 $\sigma$  dimer interface to stabilise its homodimeric form. Therefore, identifying a homodimer stabiliser for 14-3-3 $\sigma$  could potentially increase its activity and address its downregulation in cancer.

In **Chapter 2**, a literature review on the current status and outlook of drug discovery research against 14-3-3 $\sigma$ , which include the structure–activity relationship and binding interactions of the most recent 14-3-3 $\sigma$  protein-protein interaction (PPI) modulators reported to date is discussed in detail. The strategies and state-of-the-art techniques applied by various group of researchers in recent drug discovery campaign such as CADD and biophysical technologies are also discussed.

In **Chapter 3**, all general materials and methods used in this research are thoroughly described. This includes the methods used for *in silico* design, and prediction of the potential homodimer stabilisers of 14-3-3 $\sigma$ ; the synthesis, purification, and characterisation of the selected potential homodimer stabilising peptides; the expression, purification, and characterisation of the recombinant full-length 14-3-3 $\sigma$  protein; the *in vitro* interaction studies ( $^1\text{H}$ -CPMG NMR, ITC) between 14-3-3 $\sigma$  and the peptides, and the *in vitro* stabilisation studies (DLS) of 14-3-3 $\sigma$  by the selected peptide.

In **Chapter 4**, the *in silico* results on the druggability of the central cavity at the dimer interface of the 14-3-3 $\sigma$ , and the identification of the potential 14-3-3 $\sigma$  homodimer stabilising compounds from three independent approaches, i.e., virtual screening (small molecules), repositioning (GCP-Lys-OMe), and rational design (dipeptide) are described. The characterisation of the identity and purity of the synthesised compounds (dipeptides) and the recombinantly expressed full-length human 14-3-3 $\sigma$  protein were also provided in this chapter. The ability of the selected peptides to bind to the 14-3-3 $\sigma$  in *in vitro*  $^1\text{H}$ -CPMG NMR experiment was also demonstrated. The attempt to estimate the binding affinity of the best dipeptide on 14-3-3 $\sigma$  by ITC as well as the results on the thermal stability and aggregation behaviour

of  $14-3-3\sigma$  in the presence and absence of the peptide by DLS are also described in this chapter.

**Chapter 5** involves discussion on the findings described in Chapter 4. This includes a detailed discussion on the findings from each of the *in silico* design and prediction approach followed by rationalisation of the compound selection for subsequent *in vitro* binding and stabilisation studies. The key observations from the *in vitro* assays are also critically analysed and discussed in this chapter.

In **Chapter 6**, the major findings from this study are summarised. The potential limitations and future directions of this project are also discussed.

## CHAPTER 2

### LITERATURE REVIEW

#### 2.1 Introduction

The involvement of 14-3-3 $\sigma$  protein in cancer growth and metastasis have been reported in many studies, suggesting the 14-3-3 $\sigma$  as an important target for anticancer drug discovery and development. Consistent with this observation, different chemical classes of 14-3-3 $\sigma$  PPI modulators have been developed as potential therapeutics against cancer. This includes 14-3-3 $\sigma$  PPI stabilisers such as fusicocanes analogues and fragment-derived small molecule stabilisers (Section 2.2.1(a)), as well as phosphonate and non-phosphonate type 14-3-3 $\sigma$  PPI inhibitors (Section 2.2.1(b)). These modulators were successfully identified using a combination of techniques including *in silico* tools (ligand-based screening, docking, molecular dynamics simulations), biophysical techniques (NMR, X-ray crystallography, isothermal titration calorimetry (ITC), microscale thermophoresis (MST), fluorescence polarization (FP), surface plasmon resonance (SPR)), as well as cell-based assays. However, these modulators generally bind at the amphipathic pockets of the 14-3-3 $\sigma$  which are highly conserved across isoforms, thus limiting their potential use as selective anticancer agents. Thus, recent work has attempted to identify compounds targeting other site such as the dimer interface (Section 2.2.2), though the work in this area is still very limited to date.

#### 2.2 Current status and outlook of drug discovery research against 14-3-3 $\sigma$

##### 2.2.1 14-3-3 protein-protein interaction (PPI) modulators

14-3-3 PPI modulators are compounds that alter the binding affinity or specificity of 14-3-3 proteins for their target partners. These modulators can be natural

or synthetic compounds, and they can act as stabilisers or inhibitors of 14-3-3 PPIs depending on their mode of action. The modulation of 14-3-3 PPIs has been shown to have a number of biological effects, including the regulation of signal transduction, gene expression, and apoptosis, and it has been implicated in a variety of physiological and pathological processes. Therefore, 14-3-3 PPI modulators have the potential to be used as therapeutic agents for the treatment of a range of diseases, including cancer, neurodegenerative disorders, and metabolic disorders (Stevens et al., 2017; Ballone et al., 2018; Hartman and Hirsch, 2017).

### **2.2.1(a) 14-3-3 $\sigma$ PPI stabilisers**

With the increasing evidence highlighting the role of 14-3-3 $\sigma$  in suppressing cancer cell growth, metabolism, and metastasis, 14-3-3 $\sigma$  PPI stabilisation has begun to gain attention as a promising therapeutic strategy in the discovery of novel bioactive compounds against cancer. In general, PPI stabilisers work as a ‘molecular glue’ to increase the affinity of the partner protein to 14-3-3 $\sigma$  in order to achieve a positive therapeutic effect. An example of a well-studied 14-3-3 $\sigma$  PPI stabiliser is fusicoccin-A (FC-A (compound 1)) Figure 2.1a), a diterpene glycoside fungal phytotoxin which was initially found to significantly enhance the interaction between the plant analogue of 14-3-3 and the plant plasma membrane H<sup>+</sup>-ATPase (PMA2) by about 90-fold (Fullone, 1998; Würtele et al., 2003). Recently, compound 1 has been reported to be able to stabilise the interaction between 14-3-3 $\sigma$  and the tumour suppressor gene p53, as confirmed by fluorescence polarisation and isothermal titration calorimetry techniques. Nevertheless, a greater disorder in the ternary complex of 14-3-3 $\sigma$ /p53/compound 1 was observed in the crystallographic data where the C-terminus of the peptide is no longer visible (Figure 2.1b,c), suggesting that either crystal soaking may have forced the p53 peptide to form an unpreferred conformation in the presence

of compound 1 or the fact that compound 1 acts as an allosteric modulator rather than a ‘molecular glue’ in stabilising the 14-3-3 $\sigma$ /p53 interaction (Doveston et al., 2017).

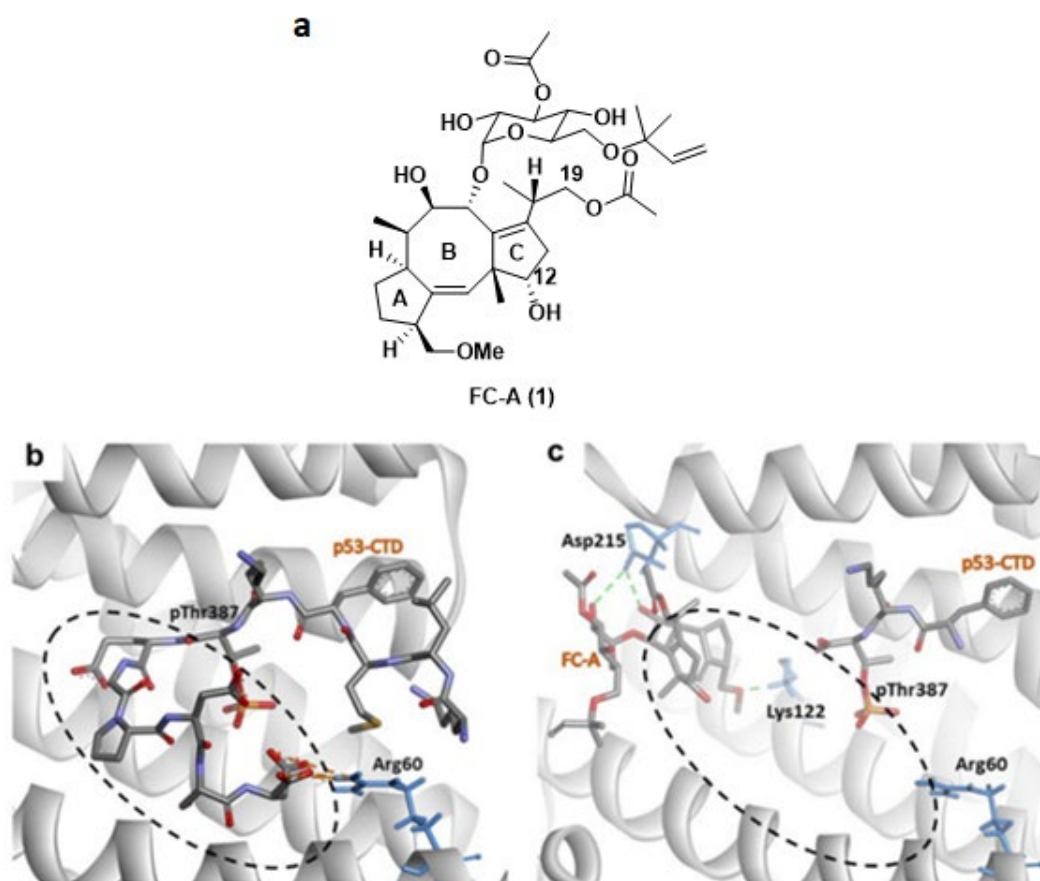


Figure 2.1 (a) Chemical structure of fusicoccin-A (FC-A). Three-dimensional (3D) crystal structure of P53/14-3-3 $\sigma$  complex (b) in the absence of FC-A (PDB: 5MOC) and (c) in the presence of FC-A (PDB: 5MXO), revealed that the C-terminus of the P53 peptide cannot be observed upon binding of FC-A (dashed circles).

Following promising results with FC-A in stabilising the interactions of 14-3-3 $\sigma$  with its protein partner, semi-synthetic analogue to compound 1, FC-THF (compound 2) (Figure 2.2a), in which a tetrahydrofuran ring was added to ring C of compound 1 was generated. However, unlike compound 1, which stabilises the interaction of 14-3-3 $\sigma$  with p53, compound 2 was found to stabilise the interaction between 14-3-3 $\sigma$  and the human potassium channel TASK-3 which is a pro-oncogenic protein that is mainly involved in cancer development. Compound 2 was reported to

be able to increase the binding affinity between TASK-3 binding motif and 14-3-3 $\sigma$  protein by up to 19-fold at 100  $\mu$ M (Figure 2.2b) (PDB: 3SMN) (Anders et al., 2013).

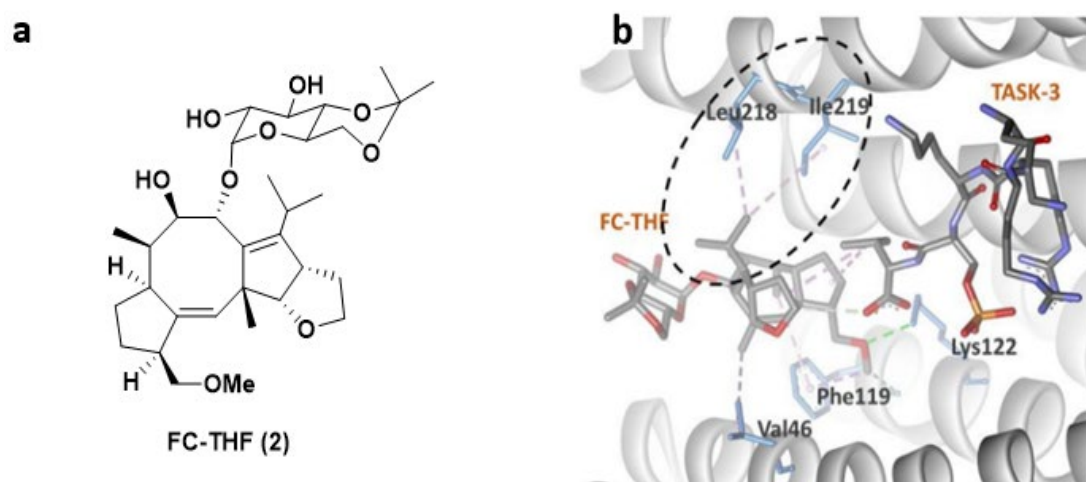


Figure 2.2 (a) Chemical structure of FC-THF. (b) 3D complex of 14-3-3 $\sigma$ /TASK-3 with FC-THF (PDB: 3SMN) revealed hydrophobic (purple dashed lines) and hydrogen bond (green dashed lines) interactions between 14-3-3 $\sigma$  and the isopropyl of FC-THF.

To further improve the affinity of fusicocanes stabilisers on 14-3-3 $\sigma$ , a series of compound 1 derivatives was designed using molecular dynamic (MD) techniques. As the conserved mode of interaction between compound 1 and 14-3-3 $\sigma$  is mainly in the form of two hydrogen bonds with Asp215 and hydrophobic interactions with Leu218 and Leu222 of 14-3-3 $\sigma$ , it was hypothesised that presenting a third hydrogen bond with Asp215 would increase the potency of the stabiliser. Therefore, the 19-acetoxy moiety of compound 1 was replaced with an isostere, 19-acetamide moiety. In addition, the 3' acetyl group which does not show a significant potency enhancement was also removed from compound 1 in order to generate a more feasible compound to synthesise. All these modifications led to compound FC-NAc (compound 3), (Figure 2.3a) which showed enhanced potency and biological activity. Further investigation into the structure of the ternary complex: 14-3-3 $\sigma$ , TASK-3 peptide, and compound 3 (Figure 2.3b) (PDB: 6GHP) revealed that Asp215 carboxylate group of 14-3-3 $\sigma$



adopted a new conformation in order to allow the formation of three hydrogen bonds with compound 3 (Andrei et al., 2018).

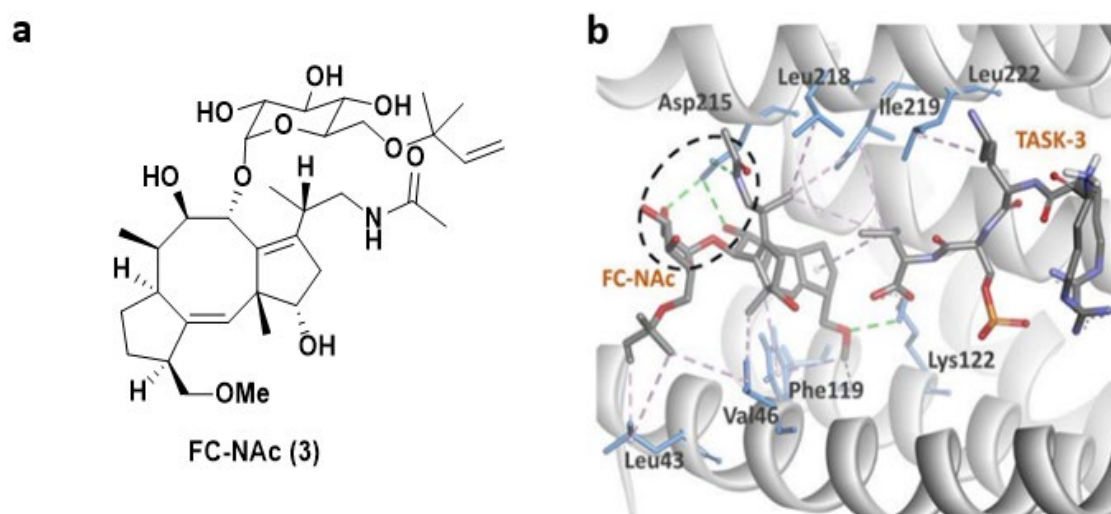


Figure 2.3 (a) Chemical structure of FC-NAc. (b) 3D complex of 14-3-3 $\sigma$ /TASK-3 with FC-NAc (PDB: 6GHP) revealed hydrophobic (purple dashed lines) and hydrogen bond (green dashed lines) interactions between 14-3-3 $\sigma$  and the 19-acetamide moiety of FC-NAc (dashed circles).

Recently, another semisynthetic analogue of compound 1, DP-005 (compound 4) (Figure 2.4a) has been reported. Unlike its predecessors which stabilise TASK-3 or p53 interactions with 14-3-3 $\sigma$ , compound 4 acts as a selective 14-3-3/p65 stabiliser. Structural elucidation of the ternary complex p65\_45R/14-3-3 $\sigma$ / compound 4 (Figure 2.4b) (PDB: 6NV2) revealed that upon binding of compound 4, p65\_45R peptide adopted a new orientation allowing compound 4 to form a hydrophobic contact via its isopropyl moiety with Ile46 and Pro47 of the peptide while it binds to Leu218, Ile219, and Leu222 of 14-3-3 $\sigma$ . This additional hydrophobic interaction with p65\_45R peptide, however, is not observed in compound 1 as the extra 12-hydroxyl group in compound 1 created a steric and polar clash with the hydrophobic residues of the peptide resulting in unpreferred interactions (Wolter et al., 2020).

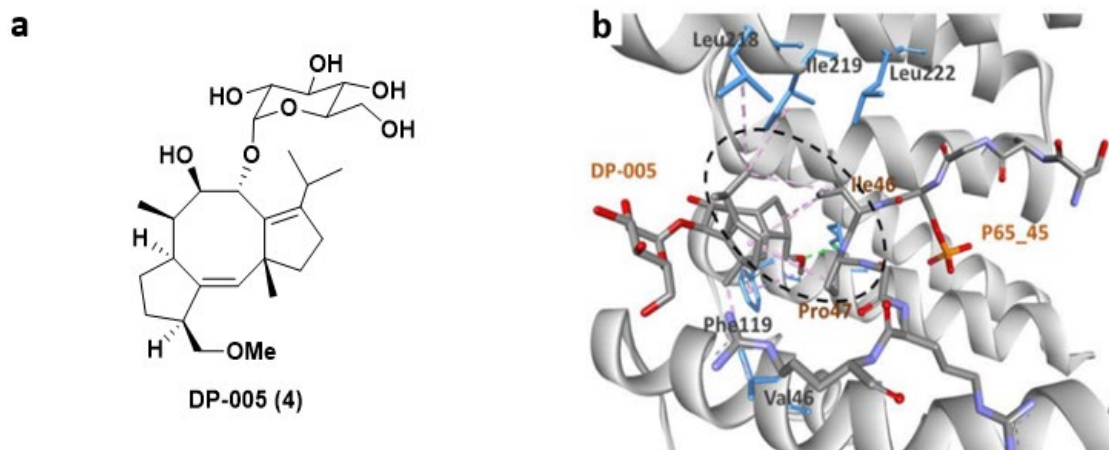


Figure 2.4 (a) Chemical structure of DP-005. (b) 14-3-3 $\sigma$ /DP-005/p65\_45R ternary complex (PDB: 6NV2) showed that DP-005 not only forms hydrophobic interactions (purple dashed lines) with 14-3-3 $\sigma$ , but also with P65\_45 (dashed circle).

Apart from the fusicocanes stabilisers, other small-molecule stabilisers of 14-3-3 $\sigma$  have also been reported. This include TCF521-123 (compound 5) and TCF521-129 (compound 6) (Figure 2.5a) which are aldehyde-containing fragment stabilisers of 14-3-3 $\sigma$ /p65 complex. Both compound 5 and compound 6 were identified using the site-directed fragment tethering approach whereby the aldehyde-bearing fragments were found to form an imine covalent anchor (instead of hydrogen bond in fusicocanes stabilisers) to the side chain of Lys122 residue at the amphipathic binding groove. Additionally, the crystallographic data obtained by crystal soaking experiments also revealed a hydrophobic interaction between the aromatic benzaldehyde ring of compound 5 and compound 6 with Ile46 of p65, while the sulphonamide group makes additional water-mediated contacts with Asn42 and Asp215 of the 14-3-3 $\sigma$ . However, while the morpholine ring of compound 6 is engaged directly with p65 peptides, the piperazine moiety of 5 is pointed away from p65 and only engaged in extra water-mediated contacts with both 14-3-3 $\sigma$  and p65 (Figure 2.5b, c). Nevertheless, both fragments are efficient stabilisers of the 14-3-3 $\sigma$ /p65 complex (Ottmann et al., 2020).

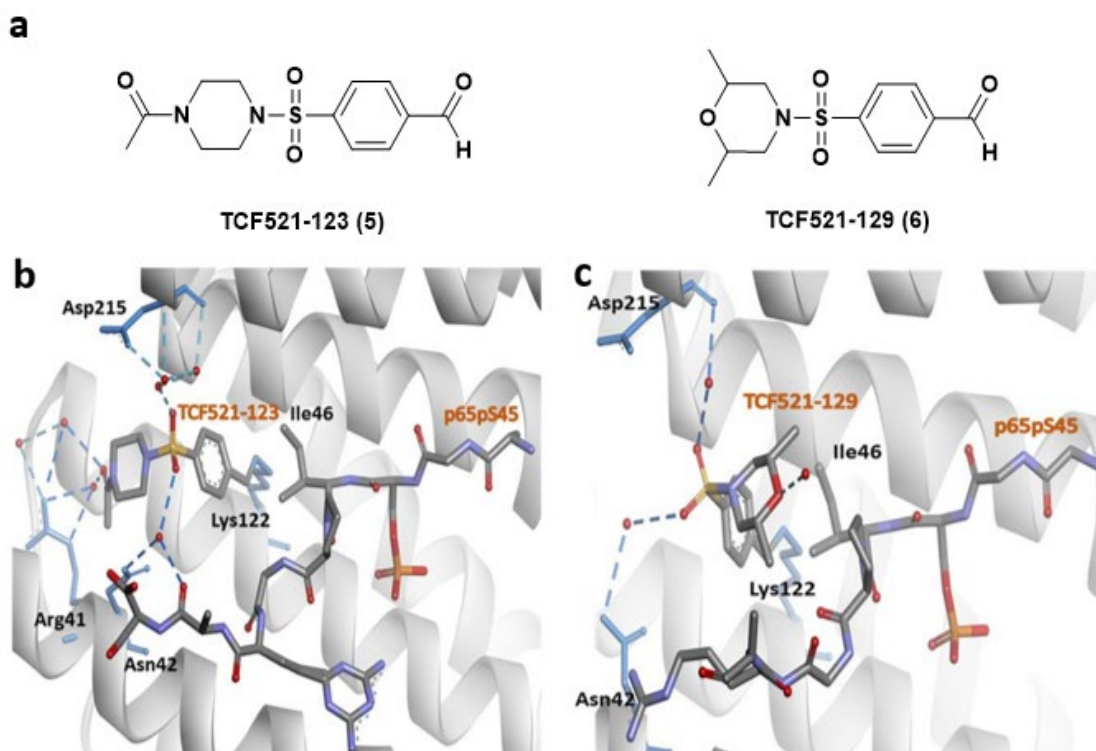


Figure 2.5 (a) Chemical structure of fragment-derived small molecule stabilisers of 14-3-3 $\sigma$  PPI. (b) 14-3-3 $\sigma$ /P65/TCF521-123 ternary complex (PDB: 6YPY). (c) 14-3-3 $\sigma$ /P65/TCF521-129 ternary complex (PDB: 6YQ2).

Using the same covalent imine-based tethering approach and by targeting the lysine residue at the interface of the composite 14-3-3 complex by an aldimine-forming fragments, a reversible covalent molecular glue for the 14-3-3 $\sigma$ /Pin1 interaction was identified from a series of an aldehyde bearing small molecules. By applying a cooperativity analysis of the ternary complex formed between 14-3-3/Pin1 and the tested small molecule, 28 (compound 7) (Figure 2.6a) was developed and found to stabilise the interaction between 14-3-3/Pin1 by more than 250-fold by selective interfacing with a unique tryptophan in Pin1. Crystal structure of 14-3-3 $\sigma$ /Pin1/compound 7 (Figure 2.6b) (PDB: 7BFW) showed the 2,4-difluorophenyl ring of compound 7 occupied a pocket formed by Cys38, Arg41, and Phe119 on the 14-3-3 $\sigma$ . This arrangement locks the orientation of the 2,4-difluorophenyl ring and cause a conformational change in the Asn42 of 14-3-3, enabling the formation of a direct

hydrogen bond with Gln of Pin1. Additionally, the Trp conformation induced by compound 7 allowed the formation of water-mediated hydrogen bonds between Trp and Gln of Pin1 and Asn42 and Ser45 of 14-3-3 $\sigma$ . Interestingly, compound 7 was found to be a selective 14-3-3 $\sigma$ /Pin1 interaction over other 14-3-3 partners targeting the same binding site such as p65 (Cossar et al., 2021).

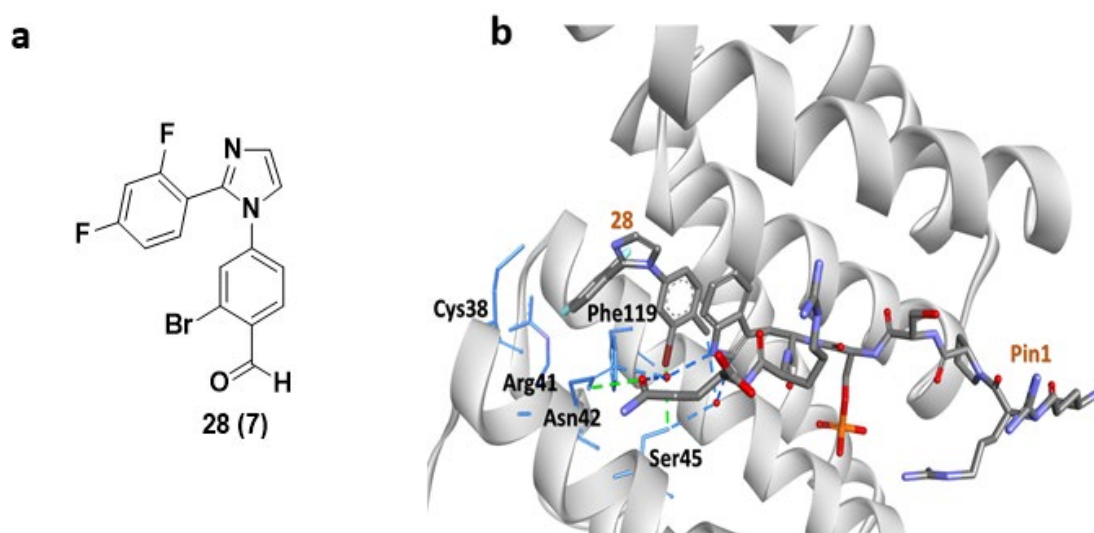


Figure 2.6 (a) Chemical structure of 28. (b) 14-3-3 $\sigma$ /Pin1/28 ternary complex (PDB: 7BFW).

Other examples of covalent small-molecule stabilisers of 14-3-3 $\sigma$  are fragment 1 (compound 8) and fragment 2 (compound 9) (Figure 2.7) which were identified using a site-directed fragment-based screening approach known as disulphide trapping. This approach utilises a cysteine on the target protein as a reactivity handle to capture disulphide-containing fragments that possess a weak intrinsic binding affinity for a target pocket near the cysteine. The bound fragments can then be detected through intact protein mass spectrometry (MS). The disulphide trapping approach was designed to target the hydrophobic pocket at the 14-3-3 $\sigma$ /ER $\alpha$  interface by binding to three 14-3-3 $\sigma$  constructs: a wildtype with a native, surface-exposed cysteine (C38) at the edge of the FC-A pocket, and two other engineered constructs in which the wildtype cysteine was mutated (C38N) and a cysteine was introduced at positions 42